الجمهـوريـــة الجزائـريـــة الديمقـراطيـــة الشـعبيـــة
République Algérienne Démocratique et Populaire
وزارة التـــعلـيـــم العـــالـــي والبـحـــث العـلمـــي
Ministère de l'Enseignement Supérieure et de la Recherche Scientifique

جامعة وهران 2 محمد بن أ حمد
Université d'Oran 2 Mohamed Ben Ahmed

معهد الصيانة و الأمن الصناعي
Institut de Maintenance et de Sécurité Industrielle

Département : Maintenance en Electromécanique

MÉMOIRE

Pour l'obtention du diplôme de Master

Filière : Electromécanique
Spécialité : Electromécanique Industrielle

Thème

Numerical Simulation of a Thermal Flat Plate Solar Collector

Présenté et soutenu publiquement par :

Salah Ajla et Aichaoui Marouane

Devant le jury composé de :

Nom et Prénom	Grade	Etablissement	Qualité
Achache Habib	MCA	Université d'Oran 2	**Président**
Dar Ramdane Mohamed Zouhir	MCB	Université d'Oran 2	**Encadreur**
Adjeloua Abdelaziz	MCA	Université d'Oran 2	**Examinateur**

Année 2023/2024

Thanks

We thank Almighty Allah for granting us health, faith, and the will to begin and complete this thesis.

First and foremost, this work would not have been as rich and could not have come to fruition without the help and guidance of our teacher and mentor, Mr. Darramdane Mohamed Zouhir. We sincerely thank him for the exceptional quality of his supervision, his patience, precision, and availability throughout our preparation of this thesis.

Our thanks also go to the president and the jury members for reviewing and showing interest in this work.

We would also like to extend our gratitude to all our professors for their generosity and great patience, despite their academic and professional commitments.

Dedication

With all pride and gratitude,I dedicate this work to my beloved mother and father, To those who have been the light of my path and my support in every step,To my siblings and friends who were by my side at every moment,

And also to the supervising professor Mr Darramdane Mohamed Zouhir , who contributed greatly to the completion of this work.

AJLA SALAH

Dedication

I dedicate this work to my dear family,To my friends who accompanied me every step of the way, And to my supervising professor Mr Darramdane Mohamed Zouhir , who spared no effort in helping me achieve this accomplishment.

Aichaoui Marouane

Abstract

This study focuses on the analysis of Flat Plate Solar Collectors (FPSC), a key technology in harnessing solar thermal energy. It combines theoretical analysis, and numerical modeling to optimize FPSC performance. Calculation model is developed to predict the thermal behavior of FPSCs using the finite difference method. In this study the impact of parameters such as mass flow rate, riser length, and solar irradiance on the system's thermal efficiency are investigated. A comparison between copper and stainless steel absorber plates is made, with copper demonstrating superior performance. The results guide the optimal design and operational strategies for maximizing thermal efficiency in FPSCs.

الملخص

تركز هذه الدراسة على تحليل مجمعات الطاقة الشمسية ذات اللوح المسطح، وهي تقنية رئيسية في استغلال الطاقة الحرارية الشمسية. تجمع الدراسة بين التحليل النظري والنمذجة العددية لتحسين أداء مجمعات الطاقة الشمسية ذات اللوح المسطح. تم تطوير نموذج حسابي للتنبؤ بالسلوك الحراري لهذه المجمعات باستخدام طريقة الفروق المحدودة. في هذه الدراسة، يتم التحقيق في تأثير العوامل مثل معدل تدفق الكتلة، وطول الأنابيب العمودية، والإشعاع الشمسي على الكفاءة الحرارية للنظام. يتم إجراء مقارنة بين الألواح الماصة المصنوعة من النحاس والفولاذ المقاوم للصدأ، حيث أظهر النحاس أداءً متفوقًا. وتوجه النتائج التصميم الأمثل والاستراتيجيات التشغيلية لتحقيق أقصى قدر من الكفاءة الحرارية في مجمعات الطاقة الشمسية ذات اللوح المسطح

Summray

List of figures

Chapter I

Chapter II

Chapter III

Nomenclature

T: Temperature (∘C)

t: Time (s)

Q: Heat quantity (J)

A: Area (m^2)

D: Diameter (m)

L: Length (m)

W: Width (m)

Cp: Heat capacity (J/Kg·K)

h: Convection coefficient ($W/m^2 \cdot C$)

V: Fluid velocity (m/s)

S: Surface area (m^2)

k: Thermal conductivity (W/K·m)

I: Incident solar radiation (W/m^2)

$\dot{m}$: Mass flow (Kg/s)

h: Enthalpy (J/kg)

$\dot{m}e$: Power radiated (W)

Greek Symbols:

α: Thermal diffusivity (m^2/s)

ρ: Density (Kg/m^3)

ϕ: Heat flow (W)

μ: Dynamic viscosity ($Pa \cdot s$)

ε: Surface emissivity

Subscripts:

T: Total

F: Fluid

Dimensionless Numbers:

Gr: Grashof number

Re: Reynolds number

Pr: Prandtl number

Nu: Nusselt number

Fo: Fourier number

Bi: Biot number

η: Efficiency

Abbreviations:

FPSC: Flat Plate Solar Collector

PTC: Parabolic Trough Collectors

HTF: Heat Transfer Fluid

SCAs: Solar Collector Assemblies

HCE: Heat Collection Elements

PCM: Phase Change Materials

FDM: Finite Difference Method

PDE: Partial Differential Equation

Indices:

I: Index of a subsequent mesh point x

J: Index of a mesh point following y

S: Solid

F: Fluid

T: Time to initial condition

I: Inlet

Mathematical Operators:

Δ: Variation

∂: Partial derivative

d/dt: Derivative with respect to time

d/dx: Derivative with respect to space

∂/∂x: Partial derivative with respect to space

∂/∂t: Partial derivative with respect to time

General Introduction

Flat plate solar collectors (FPSCs) represent a foundational technology in the realm of solar energy utilization. These collectors serve as essential tools for harnessing solar radiation for various thermal applications, ranging from heating water for domestic use to powering large-scale industrial processes.[1] FPSCs are characterized by their simple yet effective design, typically consisting of a flat absorber plate, a transparent cover (such as glass or plastic), and insulation to minimize heat losses.[2]

One of the key advantages of FPSCs is their versatility and adaptability. They can be easily fabricated and installed on rooftops, building facades, or ground-mounted structures, making them suitable for a wide range of applications and geographical locations. Additionally, FPSCs are known for their relatively low cost compared to other solar technologies, making them accessible to a broad spectrum of users. [1]

The operation of FPSCs relies on the principle of converting solar radiation into usable thermal energy. The absorber plate, typically made of a metal with high thermal conductivity, absorbs incoming sunlight and converts it into heat. This heat is then transferred to a fluid circulating within the collector, which can be water, air, or a specialized heat transfer fluid. The heated fluid can be utilized directly for heating purposes or stored for later use, providing a reliable and sustainable source of thermal energy. [3]

Over the years, extensive research and development efforts have been devoted to enhancing the efficiency and performance of FPSCs. Various modeling techniques have been developed to optimize their design, taking into account factors such as solar radiation levels, collector orientation, and heat transfer characteristics. Additionally, advancements in materials science and manufacturing processes have led to improvements in durability, reliability, and cost-effectiveness. [4]

In summary, flat plate solar collectors represent a time-tested and widely adopted technology for harnessing solar energy for thermal applications. With ongoing

advancements and innovations, they continue to play a crucial role in the transition towards a more sustainable and renewable energy future. [5]

Researchers have been refining modeling techniques to better understand and optimize the performance of FPSCs. This includes the development of computational fluid dynamics (CFD) models to simulate fluid flow and heat transfer within the collector, allowing for more accurate predictions of energy conversion efficiency and heat distribution. [6] Efforts have been made to develop novel materials and coatings for the absorber plate and cover of FPSCs to enhance their durability, heat absorption properties, and resistance to environmental degradation. For example, selective coatings with high solar absorptance and low thermal emittance have been investigated to improve the overall efficiency of the collectors. [7]

The first chapter of this study treats the operating principles and the theoretical study relating to solar collectors. In this chapter, the fundamental concepts of renewable energy, specifically solar energy, and its importance in sustainability were introduced. The focus was placed on Flat Plate Solar Collectors (FPSC), describing their components, such as absorber plates, transparent covers, and working fluids. The chapter explains how FPSCs work by absorbing solar radiation, converting it into heat, and transferring that heat to a fluid (such as water or air) that circulates through the system. The theoretical basis for solar collectors, including the different types of solar collectors based on temperature ranges, was also explored. The role of FPSCs in renewable energy was emphasized

The second chapter of this study is devoted to the literature review of the analytic, numerical and hybrid work carried out in the enhancement of flat plate solar collectors. In this chapter provided a detailed review of the existing literature on flat plate solar collectors. It covered the analytical and numerical methods used in the research of FPSCs. Analytical methods, such as the Hottel-Whillier model and Duffie and Beckman's work, were discussed, which provided a theoretical understanding of the thermal performance of FPSCs. Numerical methods, such as finite difference and computational fluid dynamics (CFD), were also explored for their ability to simulate complex heat transfer processes in FPSCs. Hybrid approaches combining analytical and numerical methods were presented as a

powerful tool for enhancing the efficiency and performance of solar collectors. This chapter highlighted the evolution of research methodologies used to optimize FPSCs

As for the third chapter, , the calculation model for analyzing the performance of FPSCs was developed. The chapter begins by discussing the various mechanisms of heat transfer (conduction, convection, and radiation) involved in the operation of an FPSC. The energy balance of the system was detailed, showing how the absorbed solar energy is distributed between useful heat gain and heat losses. Various heat transfer equations were presented to describe how energy is conducted through the collector, and convection in the fluid was modeled. Numerical methods, particularly the finite difference method, were applied to solve the complex heat transfer equations for different conditions. This chapter laid out the mathematical and computational framework used to optimize the FPSC's thermal performance

And the fourth and last chapter is devoted to the discussion of the simulation results obtained. This chapter presented the results of the numerical simulations and experiments conducted on the FPSC system under different operating conditions. The influence of key parameters like mass flow rate, riser length, and solar irradiance on the thermal performance of the system was analyzed. Results showed how varying these parameters affected the temperature distribution and thermal efficiency. The comparison between the performance of copper and stainless steel absorber plates was discussed, with copper emerging as the more efficient material for heat transfer. The chapter concluded by discussing the impact of the findings on optimizing FPSC design for higher thermal efficiency

I.1 Introduction

Renewable energy is derived from natural sources that are continually replenished for example solar energy. Unlike finite fossil fuels, which release greenhouse gases and contribute to climate change, renewable energy is both sustainable and eco-friendly. It is essential for lowering carbon emissions, combating climate change, and ensuring a sustainable energy future.

Flat plate solar collectors (FPSCs) are widely regarded as one of the most fundamental and reliable technologies for harnessing solar thermal energy. These collectors are designed to capture and convert solar radiation into heat energy, which can be used for various applications such as water heating, space heating, and industrial processes. The operating principle of FPSCs involves the absorption of sunlight by a flat absorber plate, which then transfers the generated heat to a working fluid, typically water or air, circulating through the system.[1]

Flat plate solar collectors (FPSCs) are essential in renewable energy technology. Their importance is due to several factors, including their technological simplicity, versatility, and environmental and economic advantages.[1]

This chapter describes the operating principles of a flat plate solar collectors technology, focusing more on a conventional flat plate solar collector.

I.2 Solar Collectors

Solar collectors are systems engineered to absorb solar radiation and transform it into thermal energy. This heat energy can be utilized for multiple purposes, including water heating, space heating, and electricity generation. These collectors are essential for capturing renewable solar energy, thus serving as a fundamental element in sustainable energy infrastructures.

I.2.1 Components of Solar Collectors

Absorber Material

The absorber is usually made of materials with high thermal conductivity, such as copper or aluminum, to efficiently capture solar irradiation and transfer useful heat into the working fluid .

Transparent Cover

The transparent cover, typically made of glass or plastic, covers the absorber to reduce heat loss while allowing maximum sunlight to penetrate .

Insulation:

Insulation is used to minimize heat loss from the back and sides of the collector. Common insulation materials include fiberglass, polyurethane, or mineral wool .

Working Fluid:

The working fluid, which can be water, air, or a glycol mixture, circulates through the system to transport the absorbed heat to the point of use or storage

I.2.2 Classification Based on Temperature of Solar Collector

The solar collector is the device that converts solar radiation into thermal energy through a working fluid in solar thermal applications. Solar collectors are classified based on the temperature range they achieve with the heat transfer fluid. Low-temperature solar collectors can heat the working fluid between 30–200 °C, medium-temperature collectors can heat the fluid between 200–400 °C, and high-temperature collectors are used for temperatures above 450 °C.

Figure 1, adapted from Tchanche et al. (2011) [24], illustrates the various types of solar collector technologies commonly used. Non-concentrating solar collectors, such as evacuated tube collectors (ETC), compound parabolic collectors (CPC), flat plate collectors (FPC), and advanced FPCs, heat the working fluid to temperatures below 200 °C. In contrast, concentrating solar collectors like parabolic trough collectors (PTC) and linear Fresnel reflectors (LFR) can achieve medium temperature ranges of 100-400 °C. For very high temperatures above 450 °C, dish concentrators and heliostat central receiver systems are employed. The following subsections will elaborate on the three categories of solar collectors based on their temperature ranges.

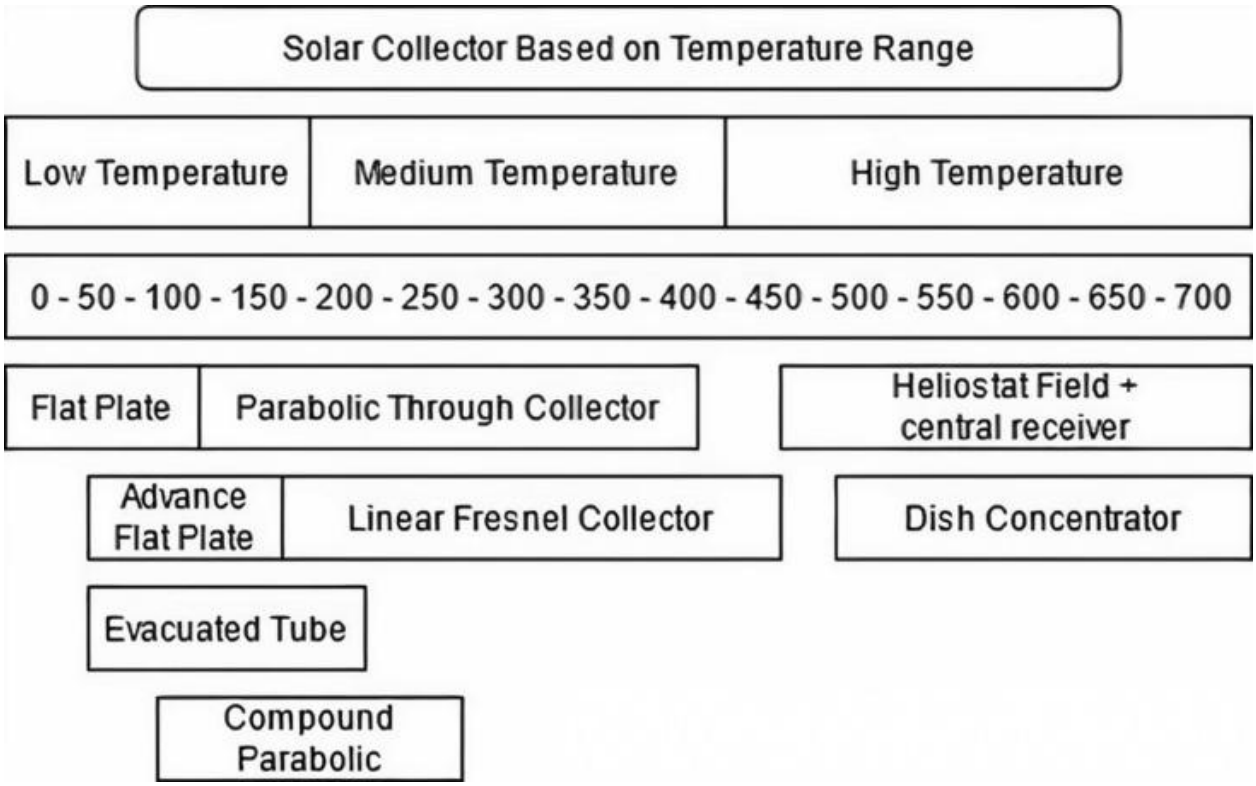

Figure 1 Solar collector application based on temperature.[25]

I.2.3 Types of Solar Collectors

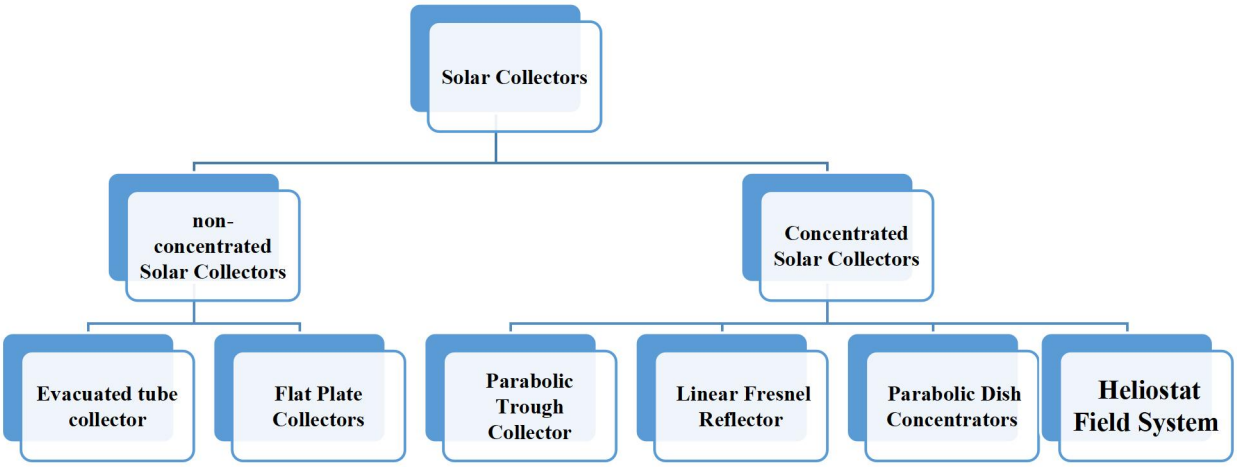

Figure 2 Classification of solar thermal collectors

I.2.3.1 Concentrated Solar Collectors

Concentrated Solar Collectors (CSCs) are advanced solar thermal technologies designed to focus sunlight onto a small area, significantly increasing the intensity of the solar energy received and thus the temperature of the working fluid. These systems are typically used for applications requiring medium to high temperatures, such as industrial process heat and electricity generation.

Parabolic Trough Collector

Parabolic Trough Collector (PTC): As illustrated in Figure II 1, medium-temperature solar collectors operate within the 200–400 °C range, including linear Fresnel collectors (LFC). Both PTC and LFC use mirror surfaces and receiver areas to concentrate and collect solar radiation, converting it into heat, and are typically classified under concentrating solar power (CSP) technologies. These systems focus solar radiation into a line.

PTCs consist of concave parabolic-shaped mirrors or reflective materials that concentrate solar rays onto a receiver tube, which absorbs the concentrated solar energy to heat the fluid inside it. This is depicted in Figure II 3, showing an integrated solar combined cycle (ISCC)

power plant in Hassi R'mel, Algeria, which utilizes PTC technology in combination with a gas source. The operating temperature of PTCs ranges from 150–400 °C, depending on the working fluid inside the tube.[25]

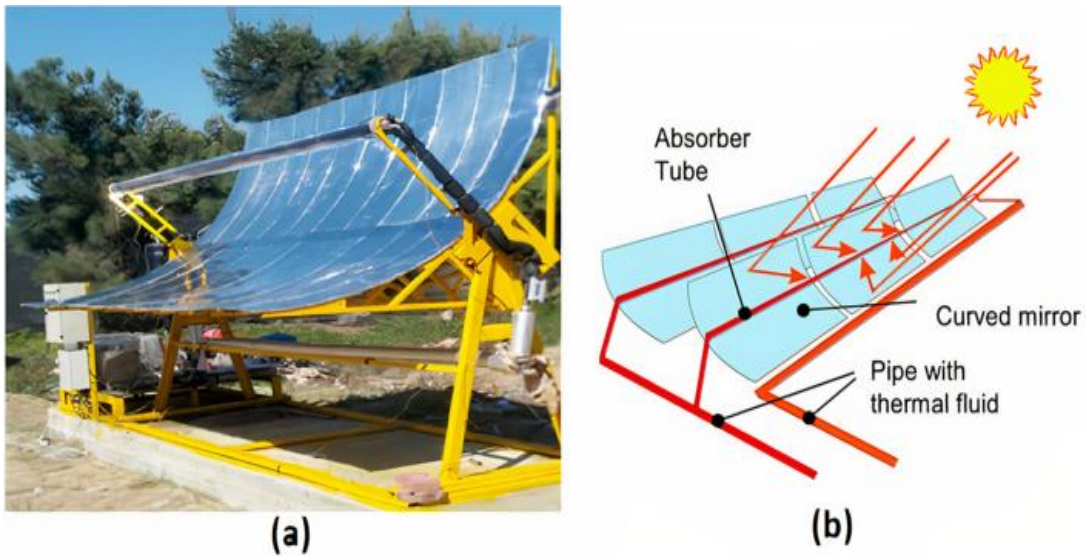

Figure 3 The solar PTC mirror [25]: (a) construction (Chafie et al., 2018) [27], (b) schematic (Romero and González-Aguilar, 2013) [28]

Achour et al. (2018) [29] evaluated the performance of the ISCC. Their analysis revealed that during sunny periods, the solar-to-electricity efficiency could reach up to 14.4%, with an overall thermal efficiency of about 60%, which are considered feasible values. Additionally, the previous discussion highlighted that the working fluid impacts PTC performance..[25]

Linear Fresnel Reflector (LFR)

The Linear Fresnel Reflector (LFR) is a type of solar collector that also uses mirror surfaces to concentrate sunlight and convert it into heat. Unlike Parabolic Trough Collectors (PTCs), which have a continuous parabolic-shaped reflector, LFRs consist of numerous long mirror strips that can be independently adjusted (single-axis tracking) to reflect solar radiation onto an absorber. The concentration ratio for LFRs typically ranges from 10% to 50%. A typical image of an LFR is shown in Figure 4.

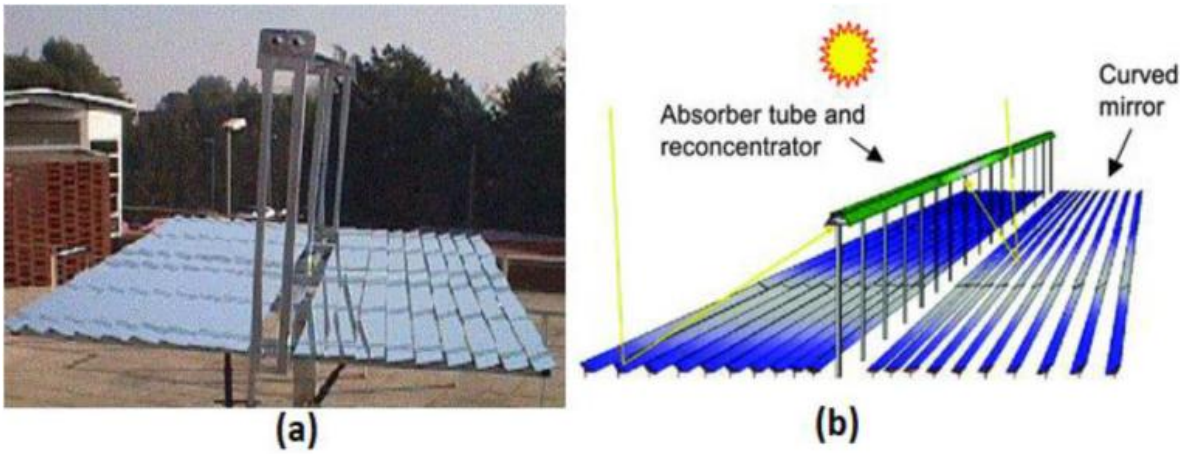

Figure 4 LFR[25]: (a) construction (Rosell et al., 2005)[31], (b) schematic (Romero and González-Aguilar, 2013).[28]

Generally, LFRs use water as the standard working fluid to produce saturated or superheated steam (150–450 °C). This steam can be directly utilized to drive turbines in a conventional Rankine cycle for electricity generation or for industrial processes. Additionally, some research explores the use of molten salts, as demonstrated by Grena and Taquini (2011)[32], who analyzed the use of molten nitrates as a heat transfer fluid in LFRs and outlined the system's advantages and disadvantages. Bellos et al. (2018)[33] compared three working fluids (thermal oil, molten salt, and liquid sodium) for LFRs through optical and thermal analysis, finding liquid sodium to be the most effective. Both PTC and LFR

technologies are promising, and advancements in solar concentrator technologies could significantly enhance solar power generation in the coming decades.[25]

Parabolic Dish Concentrators (PDC)

Parabolic Dish Concentrators (PDC) are a type of solar thermal collector that utilizes a parabolic dish-shaped reflector to concentrate sunlight onto a focal point where a receiver is located. This concentrated solar energy is then converted into thermal energy, which can be used for various applications, including electricity generation and high-temperature industrial processes a typical image of a PDC is shown in Figure 5.

Recent research and development in PDC technology have focused on improving efficiency, reducing costs, and enhancing durability. For example, advanced materials and coatings are being developed to increase the reflectivity and longevity of the dish's surface. Additionally, innovative cooling and heat transfer techniques are being explored to improve the performance of the receiver.[35]

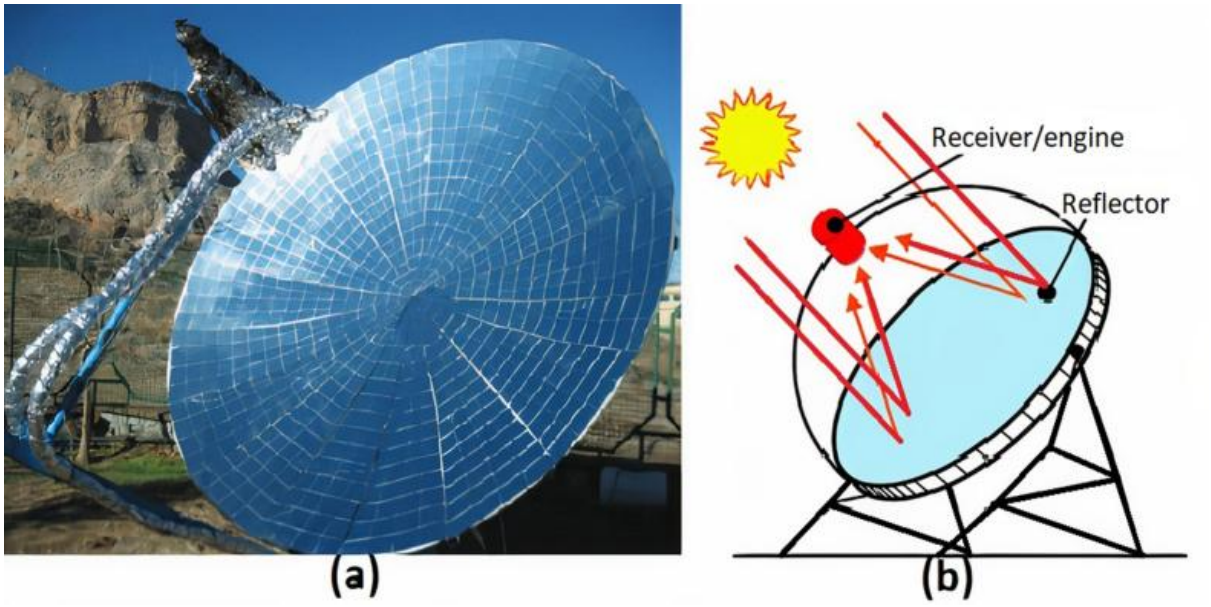

Figure 5 (a) construction (Madadi et al., 2014)[36], (b) schematic (Romero and González-Aguilar, 2013)[28].

Heliostat Field System

A Heliostat Field System is a key component in central receiver solar power plants, also known as solar tower plants (Figure 6). This system consists of numerous heliostats-mirrors that track the sun on two axes and reflect sunlight onto a central receiver located atop a tower. The concentrated solar energy collected by the receiver is then converted into thermal energy, which can be used to generate electricity or for other thermal applications. The system of heliostat has a concentration ratio from 300 to 1500 and the temperature range between 200–2000 °C (Rabbani et al., 2017). [37]

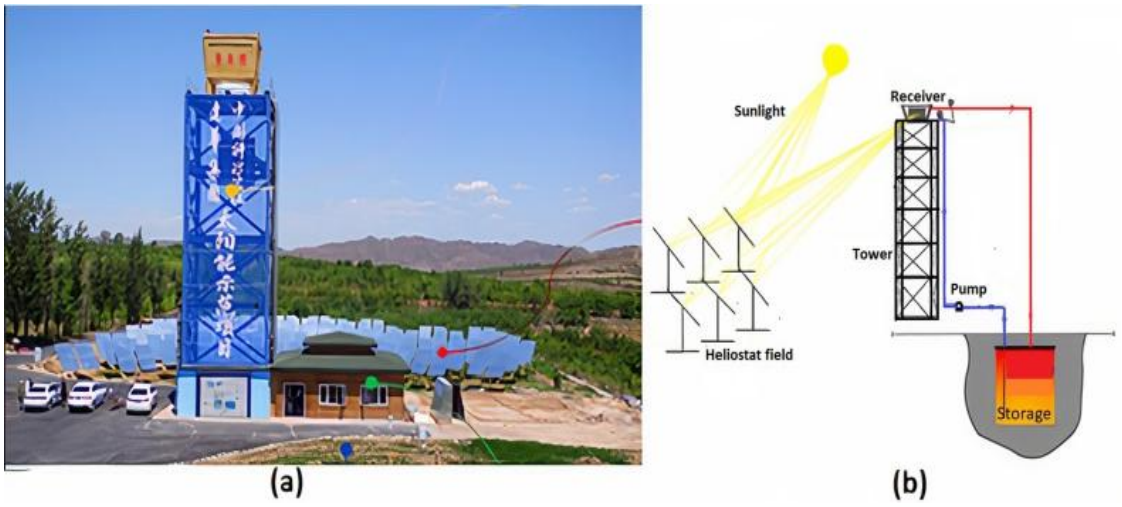

Figure 6 Heliostat field and receiver: (a) construction[39], (b) schematic (Li et al., 2021)[40].

I.2.3.2 Non-concentrated Solar Collectors

Evacuated Tube Collector

Evacuated Tube Collectors (ETCs) are a type of solar thermal collector designed to capture solar energy and convert it into heat. These collectors consist of multiple glass tubes, each containing an absorber plate or fin. The space inside the tubes is evacuated to create a vacuum, which significantly reduces heat loss by minimizing conduction and convection.[39]

As illustrated in Figure 7, a heat pipe is connected to the absorber plate. Inside the heat pipe, a working fluid undergoes evaporation and condensation, facilitating heat transfer between the heat pipe condenser and the heat transfer fluid. The collector material heats the fluid inside the heat pipe until it evaporates. The vapor then rises to the top, where it condenses due to the cooler conditions in the manifold, releasing latent heat in the process. The vacuum insulation in the ETC effectively minimizes heat loss to the environment, allowing the internal temperature within the tube to reach up to 423 K, while the external surface remains at ambient temperature. [40]

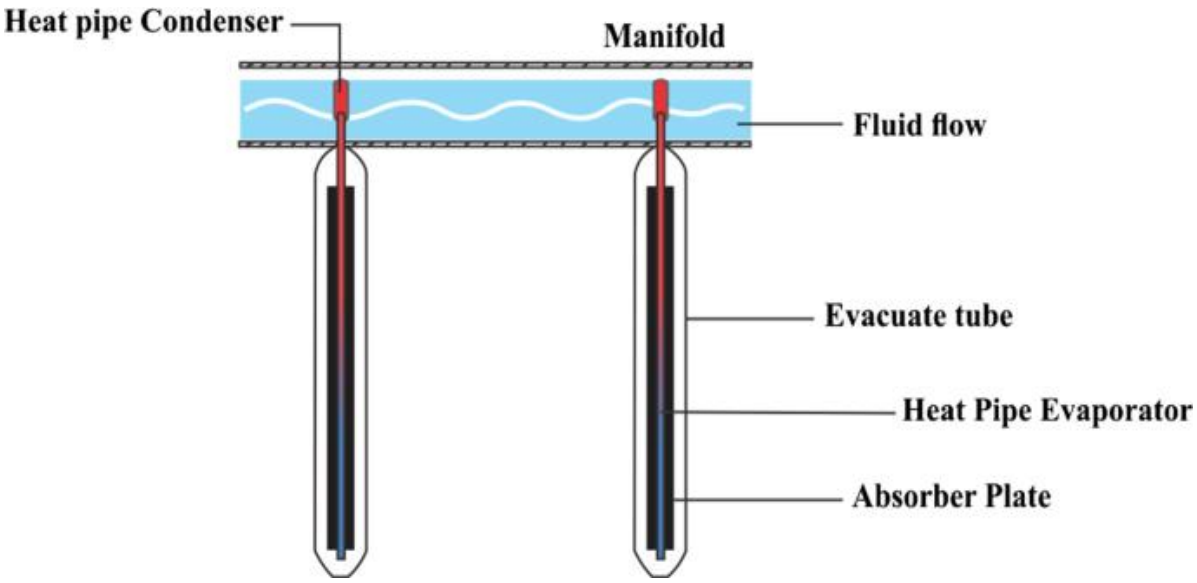

Figure 7 Diagram of a heat pipe evacuated tube collector (ETC)[40]

Flat Plate Collectors (FPCs)

Flat Plate Collectors (FPCs) are extensively used for capturing solar thermal energy. These devices feature a flat metal absorber plate, which is coated with a material that boosts its solar radiation absorption capabilities. A transparent cover (glazing) is placed over the absorber plate to diminish heat loss, while the back and sides are insulated to further reduce thermal losses. Water or another heat transfer fluid flows through tubes connected to the absorber plate, absorbing the heat and carrying it to be used in different applications.[41]

The heat absorbed by the absorber plate is conveyed to the working fluid (air, water, etc.) in the risers (pipes) through convective heat transfer. The diagram of the flat plate collector is depicted in Figure II 9.

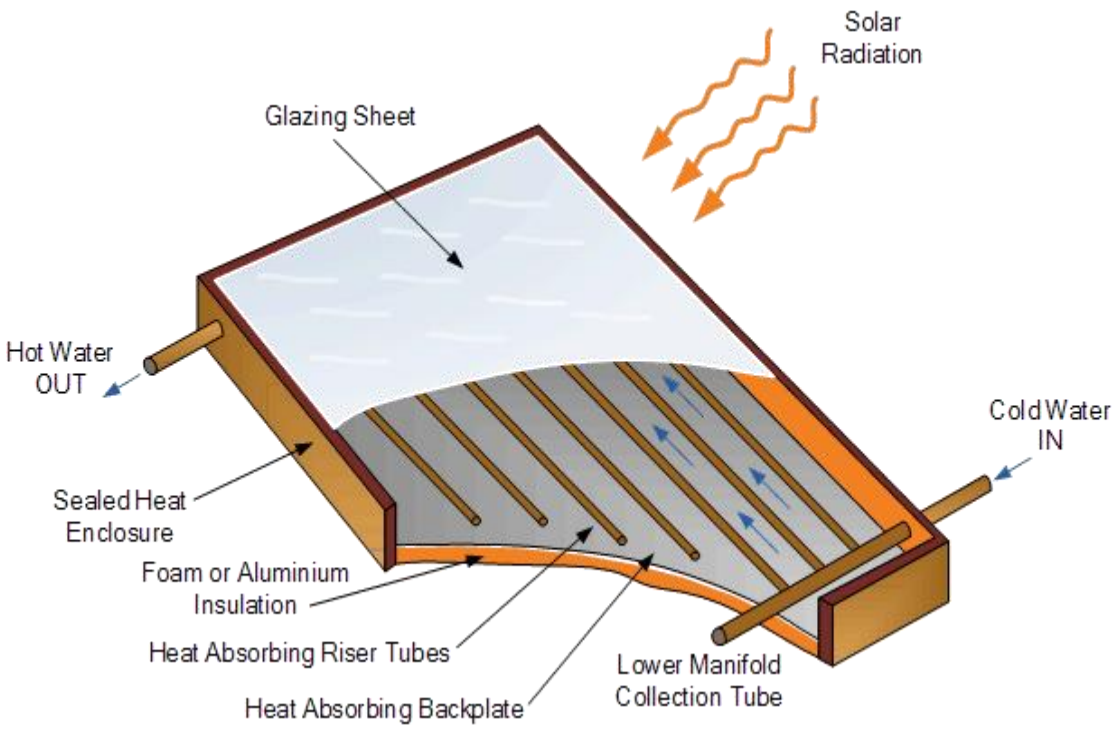

Figure 8 Diagram of a Flat Plate Collector[40]

The primary components of a flat plate collector (Figure II 9) include:

Cover: One or more sheets of glass or other materials that transmit radiation.

Heat removal fluid passageways: Tubes, fins, or passages that direct the heat transfer fluid from the inlet to the outlet.

Absorber plate: Flat, corrugated, or grooved plates to which the tubes, fins, or passages are attached. This plate is typically coated with a high-absorptance, low-emittance layer.

Headers or manifolds: Pipes and ducts used to admit and discharge the fluid.

Insulation: Material used to minimize heat loss from the back and sides of the collector.

Container: The casing that surrounds and protects the components from dust, moisture, and other materials.[43]

I.2.4.1 Thermal Insulation

Thermal insulation is crucial for the performance and efficiency of solar collectors (SCs) for several reasons.

Firstly, it reduces heat losses from the absorber plate to the surroundings, retaining the heat within the system and maximizing its effectiveness in converting solar radiation into usable thermal energy.

Secondly, insulation maintains the necessary temperature differentials for efficient heat transfer within the SC by allowing the absorber plate to remain at a higher temperature relative to the ambient environment.

Thirdly, effective insulation enhances the thermal efficiency of SCs by minimizing energy losses during the heat transfer process, resulting in a higher proportion of captured solar energy being utilized for heating purposes.

Lastly, insulation improves the performance of SCs under varied environmental conditions by ensuring consistent performance and thermal output despite fluctuating solar radiation levels and ambient temperatures.

I.3.1 Operating Principle

Flat Plate Solar Collectors (FPSCs) function by absorbing solar radiation through a selectively coated absorber plate, which then transfers the generated heat to a working fluid flowing through tubes or channels.

This process begins with solar radiation passing through a transparent cover and striking the absorber plate, which is designed to maximize absorption and minimize heat loss. The heated absorber plate by radiation heat transfer located beneath the cover usually made of metal (such as copper or aluminum) and coated with a selective material that has high solar absorptance and low thermal emittance.

The heat generated in the absorber plate is then transferred to the working fluid (which could be water, antifreeze solution, or air) flowing through tubes or channels (risers) attached to or integrated within the absorber plate. This transfer of heat is primarily through conduction and convection.

The fluid enters the collector through an inlet manifold, travels through the risers where it picks up heat, and exits through an outlet manifold. Headers and manifolds facilitate the distribution and collection of the fluid across the entire absorber plate.

This fluid, heated by the collector, is circulated using either a pump or natural convection for various applications such as water heating, space heating, or industrial processes. Alternatively, the heat can be stored in a thermal storage system for later use.

To enhance efficiency, the collector is insulated at the back and sides to prevent heat loss, while the transparent cover helps reduce convective and radiative losses.

The overall design ensures efficient capture and transfer of solar energy, making FPSCs a reliable and widely used technology in solar thermal systems.

I.4 Conclusion

This chapter provided an overview of existing research on Solar collectors and there operating principal , such as Flat Plate Collectors (FPCs), Evacuated Tube Collectors (ETCs), Parabolic Trough Collectors (PTCs), Linear Fresnel Reflectors (LFRs), and

Parabolic Dish Collectors (PDCs). Each type has unique features and uses, suitable for a range of temperature needs from low to high, and is applied in residential, commercial, and industrial settings.

Investing in solar energy is worthwhile, and it will lead to complete energy independence and numerous other benefits. Despite some drawbacks, most issues can be addressed with appropriate solution

II.1 Introduction

Flat Plate Solar Collectors (FPSC) are integral components in the field of solar thermal energy systems, designed to capture and convert solar radiation into usable heat energy. The performance and efficiency of FPSCs depend heavily on their design and operational parameters, which necessitate the use of accurate calculation models. These models are essential for predicting the thermal behavior, optimizing the design, and enhancing the overall efficiency of the collectors.

Calculation models of FPSCs typically incorporate a combination of heat transfer mechanisms, including conduction, convection, and radiation, to provide a comprehensive analysis of the energy balance within the system. The primary objective of these models is to determine the temperature distribution across the collector, the heat gain by the working fluid, and the overall thermal efficiency.

A typical calculation model begins with the formulation of energy balance equations that account for the solar energy absorbed by the collector, the heat losses to the environment, and the heat transferred to the working fluid. These equations are derived based on the principles of thermodynamics and heat transfer, incorporating factors such as the properties of the absorber plate, the glazing material, the insulation, and the working fluid.

The calculation process involves solving these energy balance equations, often requiring numerical methods due to the complexity of the interactions between different components of the collector. Advanced computational tools and simulation software are employed to handle the non-linearities and transient behaviors inherent in the system were 2D model calculations carried out through partial differential equations..

Overall, the development and utilization of calculation models are crucial for the design, optimization, and performance evaluation of Flat Plate Solar Collectors. They provide valuable insights that guide engineers and researchers in improving the technology to meet the growing demand for sustainable and efficient solar energy solutions.

II.2 Heat Transfer Review

In thermodynamic terms, heat transfer refers to the flow of thermal energy across the system's boundary caused by a temperature disparity between the system and its surroundings [22]

II.2.1 Heat Flux

Heat circulates from high to low temperatures due to a temperature gradient and it refers to the process by which thermal energy is exchanged between different objects or systems due to a temperature difference. This exchange can occur through three primary mechanisms:

Conduction: Heat transfer through direct contact between objects or particles. In conduction, thermal energy is transferred from regions of higher temperature to regions of lower temperature through molecular collisions(Figure III 1).

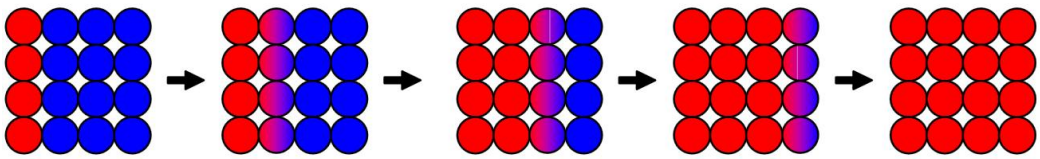

Figure II 1: Heat transfer by conduction

The rate of conduction depends on the thermal conductivity of the material, the temperature difference, and the cross-sectional area through which heat flows.

In the case of a wall, one dimensional heat transfer rate is described by Fourier's law of heat conduction as:

$$q=-KA\frac{dT}{dx} \qquad \text{II 1}$$

Convection: Heat transfer through the movement of fluids (liquids or gases). Convection occurs when warmer fluid molecules move from regions of higher temperature to cooler regions, carrying thermal energy with them.

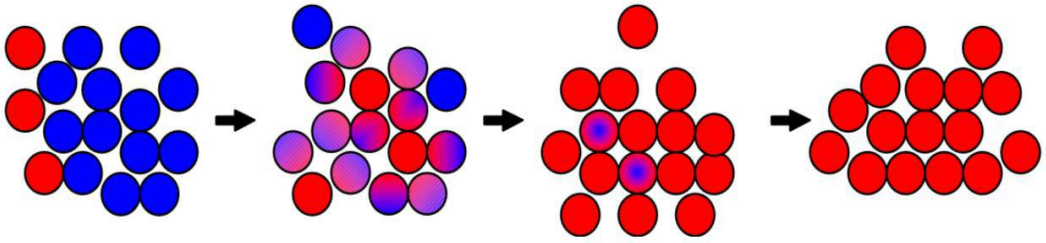

Figure II 2 Heat transfer by convection

The rate of energy transfer from the surface to the fluid can be quantified by Newton's law of convection as:

$$q=A.h.(T_S-T_\infty) \qquad \text{II 2}$$

Natural Convection

Heat transfer by natural convection occurs when a body is placed in a fluid with a different temperature than the body. This temperature difference causes heat to flow between the fluid and the body, resulting in a change in the density of the fluid near the surface.[44]

The natural movement of fluids is described by the dimensionless Grashof number:

$$\mathrm{Gr} = \frac{gL^3\beta\Delta T\rho^2}{\mu^2} \qquad \text{II 3}$$

Forced Convection

In forced convection, fluid moves rapidly over the surface, typically driven by a pump for liquids or a fan or blower for gases.[45]

The experimental data for forced convection are correlated through the use of three dimensionless numbers:

- The Reynolds number Re.

$$\mathrm{Re} = \frac{\rho VD}{\mu} \qquad \text{II 4}$$

Were ρ,V,D, μ is the fluid density and velocity and the diameter of riser or manifold and dynamic viscosity respectively

- The Prandtl number Pr.

$$\mathrm{Pr} = \frac{C_p \mu}{K} \quad \text{II 5}$$

Were C_p and K is the specific heat and thermal conductivity respectively

- The Nusselt number Nu.

$$\mathrm{Nu} = \frac{hD}{K} \quad \text{II 6}$$

Were h is the heat transfer coefficient

The correlation of the experimental data gives the Nusselt number as a function of the other numbers:

$$Nu=(Re,Pr,Gr) \quad \text{II 7}$$

Once the Nusselt number is determined, the convective coefficient can be obtained from the definition of Nusselt number given in equation II 6.

Radiation: Heat transfer through electromagnetic waves, such as infrared radiation. Unlike conduction and convection, radiation does not require a medium to propagate and can occur across a vacuum.

All objects emit thermal radiation based on their temperature. According to the Stefan-Boltzmann law, the rate of heat transfer through radiation is proportional to the fourth power of the absolute temperature.

$$\dot{Q}_e = \varepsilon \sigma \mathrm{A} T_b^4 \quad \text{II 8}$$

With $\sigma = 5.64 \times 10^{-8}\, {}^{W}/_{m^2 K^4}$

II.2.2 Flow Regimes

Flow regimes are classifications of fluid flow based on the flow's behavior. The common classification is based on the Reynolds number.

The three main flow regimes are in Figure II 3:

Laminar flow: This type of flow is smooth and orderly, with fluid layers moving parallel to each other. It occurs at low Reynolds numbers (Re < 2300), where viscous forces dominate.

Turbulent flow: This type of flow is chaotic and irregular. It occurs at high Reynolds numbers (Re > 3000), where inertial forces dominate and the flow becomes turbulent.

Transitional flow: This flow occurs in the intermediate range of Reynolds numbers (2300 < Re < 3000), where the flow behavior is unstable and can switch between laminar and turbulent regimes.

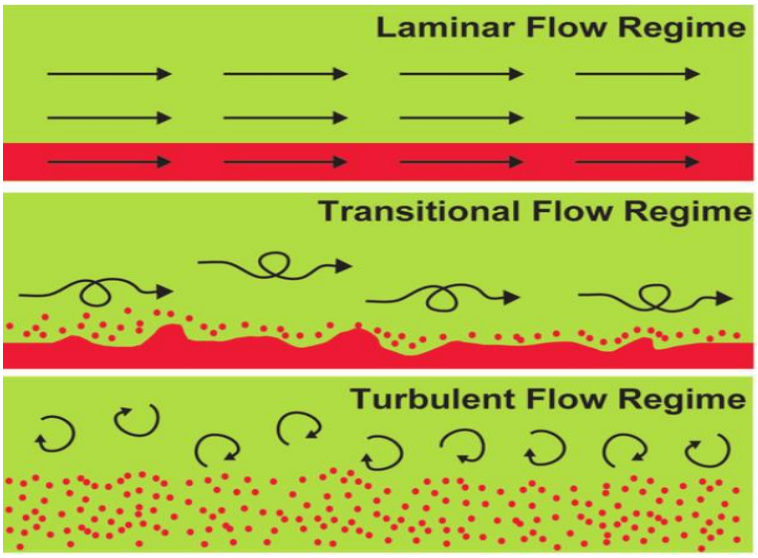

Figure II 3: The flow regimes.

II.2.3 Fluid Temperature in a Tube with Constant Wall Temperature

As heat is transferred through the tubes, the fluid temperature increases. Because the solid temperature is higher than the fluid temperature, the fluid absorbs heat from it. Figure III 4 illustrates an analysis of internal convection in the fluid with a constant tube surface temperature.

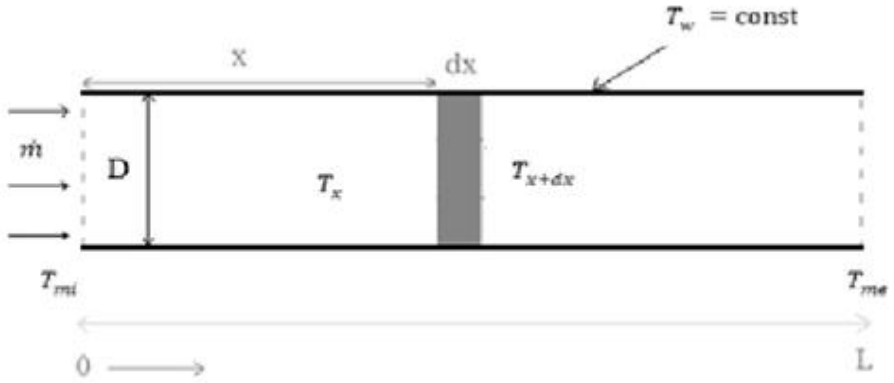

Figure II 4: Internal convection in tube with constant surface temperature.

$$(\pi \mathrm{Ddx})\mathrm{h}(\mathrm{Tw}-\mathrm{Tx}) = \dot{m}c_p(T_{x+dx} - T_x) \qquad \text{II 10}$$

With $T_{x+dx} = T_x + dT_x$; $\dot{m} = \rho AV$ and $= \frac{\pi D^2}{4}$; (πDdx) is convection area

$$(\pi \mathrm{Ddx})\mathrm{h}(\mathrm{Tw}-\mathrm{Tx}) = \dot{m}c_p(T_x + dT_x - T_x)$$

$$\int_{x=0}^{x} \frac{\pi Dh}{\dot{m}c_p} dx = \int_{T_{mi}}^{T_x} \frac{1}{(\mathrm{Tw}-\mathrm{Tx})} dT_x$$

Becomes $-\frac{\pi Dhx}{\dot{m}c_p} = ln(\mathrm{Tw}-\mathrm{Tx}) - ln(\mathrm{Tw}-\mathrm{Tmi})$

$$\ln\frac{(T_x - T_w)}{(T_{mi} - T_w)} = -\frac{\pi Dhx}{\dot{m}c_p}$$

$$(T_x) = (T_{mi} - T_w)e^{-\frac{\pi Dhx}{\dot{m}c_p}} + T_w \qquad \text{II 11}$$

The equation II.11 represents how the temperature at a certain point within the fluid changes due to the combined effects of heat conduction and convection into or out of the fluid.

II.2.4 Heat Transfer Mechanisms in Solar Collectors

Conduction

Heat conduction takes place in the absorber plate and through the insulation materials. The efficiency of heat conduction affects how well the absorbed solar energy is transferred to the working fluid.[1]

Convection

Natural Convection: Occurs in the air gap between the absorber plate and the glazing. It also happens in the fluid passages if the system is not pump-driven.

Forced Convection: Typically occurs in the fluid transport system where pumps circulate the working fluid through the absorber plate pipes or tubes.[5]

Radiation

The absorber plate absorbs solar radiation and re-emits infrared radiation. The glazing material transmits the incoming solar radiation and reduces the re-radiation loss from the absorber plate to the environment[23]

II.3 Energy Balance

The energy balance in an FPSC is crucial for its performance optimization. It involves calculating the total solar energy input, the useful energy output, and the various heat losses. The energy input is determined by the incident solar irradiance and the collector area. The useful energy output is the amount of absorbed solar energy converted into heat and transferred to the working fluid. Energy losses occur through conduction, convection, and radiation, which are collectively represented by a heat loss coefficient.

II.3.1 Components of Energy Balance in FPSCs

Solar Energy Input:

The amount of solar radiation incident on the collector surface is the primary input. This can be represented as $Qsolar=I\cdot A_c$, where I is the solar irradiance (W/m²) and A_c is the collector area (m²).

Absorbed Energy:

Not all incident solar radiation is absorbed. The efficiency of absorption depends on the properties of the absorber plate and the glazing. The absorbed energy can be represented as $Qabs= \tau\alpha \cdot Q$, where $(\tau\alpha)$ is the absorptance-transmittance product of the glass cover and the absorber plate.

Thermal Losses:

Heat losses occur through conduction, convection, and radiation. These losses can be expressed as

$$Qloss=Qcond+Qconv+Qrad \quad \text{II 11}$$

Conduction Losses: Occur through the insulation materials.

Convection Losses: Occur due to the air gap between the absorber plate and the glazing,and from the surface to the ambient environment.

Radiation Losses: Occur from the absorber plate to the surroundings.

Useful Heat Gain

The useful heat gain by the working fluid is the amount of absorbed energy minus the thermal losses. This can be represented as

$$\text{Quseful} = A_c\left[\tau\alpha I - U_L(T_p - T_a)\right] \qquad \text{II 12}$$

Where, Quseful is the useful energy rate; A_c is the FPC area; $(\tau\alpha)$ is the absorptance-transmittance product; I is the incident solar irradiation; T_a and T_p are ambient and absorber plate temperature, respectively and U_L is the overall heat loss coefficient.

Overall heat loss coefficient

Top heat loss coefficient

The heat transfer coefficient by convection from the absorber plate to the cover h_{1c} can be written as follows:

$$h_{1c} = \frac{NuK_f}{L_f} \qquad \text{II 13}$$

Where K_f and L_f are the fluid thermal conductivity and the spacing between absorber plate and transparent cove, respectively.

The heat transfer coefficient by radiation from the absorber plate to the cover $h_{1r}$is given as follows:

$$h_{1r} = \varepsilon_{eff}\sigma\frac{T_p^4 - T_g^4}{T_p - T_g} \qquad \text{II 14}$$

where $\sigma = 5.64 \times 10^{-8}\, W/m^2K^4$ is Stefan's constant. The ε_{eff} is the effective emissivity of plate-glazing system, and it is given by:

$$\varepsilon_{eff} = \frac{1}{\left[\frac{1}{\varepsilon_p}+\frac{1}{\varepsilon_g}-1\right]} \qquad \text{II 15}$$

The heat transfer coefficient by convection from the cover to the ambient h_{2c} is calculated by Watmuff et al. (1977) correlation.

$$h_{2c} = 2.8 + 3V_{wind} \qquad \text{II 16}$$

Here V_{wind} is wind speed over the collector transparent cover.

The heat-transfer coefficient for radiation from a glass cover to the ambient environment is influenced by the long-wavelength radiation exchange with the sky at the sky temperature Tsky. This relationship can be expressed as follows:

$$T_{sky} = T_a - 6 \qquad \text{II 17}$$

Thus, the radiative heat-transfer coefficient, h2r , can be written as follows:

$$h_{2r} = \varepsilon_{eff}\sigma\frac{T_g^4 - T_{sky}^4}{T_g - T_a} \qquad \text{II 18}$$

The top heat loss coefficient U_t is expressed as:

$$U_t = \frac{1}{\left[\frac{1}{h_{1r}+h_{1c}}+\frac{1}{h_{2r}+h_{2c}}\right]} \qquad \text{II 19}$$

Back-loss coefficient

Heat is lost from the absorber plate to the ambient air by conduction through the

Insulation expressed as:

$$U_b \approx \frac{K_i}{L_i} \qquad \text{II 20}$$

Where K_i and L_i are the insulation conductivity and thickness respectively

The overall heat loss coefficient U_L is the summation of the top and back heat loss coefficients.

$$U_L = U_t + U_b \qquad \text{II 21}$$

Energy Transferred to Working Fluid

The energy transferred to the working fluid (water) is what is ultimately used for heating or other applications. This is the useful heat gain transferred through the collector pipes or tubes.

Mathematical Formulation of Energy Balance

The energy balance equation for a flat plate solar collector can be formulated as equation II-12

$$\text{Quseful} = A_c\left[\tau\alpha I - U_L(T_p - T_a)\right]$$

Where: $Quseful$ is the useful heat gain, $(\tau\alpha)$ is the absorptance-transmittance product, I is the solar irradiance, A_c is the collector area, U_L is the overall heat loss coefficient, $Qcond$ represents the conduction losses, $Qconv$ represents the convection losses and $Qrad$ represents the radiation losses.

This equation highlights the importance of optimizing the properties of the absorber plate, improving insulation, and minimizing heat losses to maximize the efficiency of the solar collector.

II.3.2 Defining Heat Transfer Problem

Defining a heat transfer problem involves several key steps to ensure a comprehensive understanding and accurate analysis. Here are the main components:

Identify the System and Boundaries: Clearly define the physical system under study and its boundaries. This includes specifying the geometry, material properties, and the region where heat transfer occurs.

Determine Heat Transfer Modes: Identify the modes of heat transfer present in the system—conduction, convection, and radiation. Each mode has its own governing equations and assumptions.

Specify Initial and Boundary Conditions: Define the initial temperature distribution within the system and the boundary conditions. Boundary conditions can include constant temperature, convective heat transfer, radiation, or a combination of these.

Formulate Governing Equations: Develop the mathematical models that describe the heat transfer processes within the system. These equations are typically partial differential equations (PDEs) representing energy conservation in terms of heat flux, temperature gradients, and material properties.

Determine Material Properties: Obtain the necessary thermal properties of the materials involved, such as thermal conductivity, specific heat capacity, and emissivity. These properties can vary with temperature and need to be accurately defined for the analysis.

Simplify the Problem (if possible): Make appropriate assumptions to simplify the problem without compromising the accuracy of the results. Common assumptions include steady-state conditions, one-dimensional heat flow, or neglecting minor heat transfer modes.

Solve the Equations: Apply numerical methods to solve the governing equations with the specified initial and boundary conditions. Numerical methods (such as finite element analysis) are used for more complex problems.

II.4 Numerical Methods in Two-Dimensional and Transient Regimes

Numerical methods for heat transfer problems have been in use since at least the 1940s. With the widespread adoption of digital computers in the 1960s and 1970s, researchers and students gained the ability to tackle problems that were extremely difficult or impossible to solve analytically.[46]

Several numerical methods are utilized in heat transfer, such as finite difference, finite element, and finite volume methods. This discussion focuses extensively on the finite difference method, which is subsequently applied to solve a two-dimensional unsteady-state problem.

II.4.1 Finite Difference Method

The finite difference method (FDM) is a numerical approach for approximating solutions to differential equations, particularly partial differential equations (PDEs). It involves discretizing the spatial and occasionally temporal domains into a grid of points and approximating derivatives through finite differences. This technique is extensively applied across diverse fields, including heat transfer, fluid dynamics, electromagnetism, and finance.

The finite difference method is employed to address the direct problem of two-dimensional heat conduction in an unsteady state, without an internal heat source, and to analyze the temperature distribution of the flowing fluid.

II.4.1.1 Discretization of the Domain

The first step in using the finite difference method (FDM) is to discretize the spatial and temporal domains of the problem. This means dividing the domain into a grid of discrete points. In one dimension (1D), the domain is divided into intervals, while in two dimensions (2D) or three dimensions (3D), a grid or mesh is created.

II.4.1.2 Formulation of Discrete Equations

By employing finite difference approximations, it becomes straightforward to convert the original differential equations into a series of discrete equations. These equations usually

consist of algebraic equations that establish the relationship between the values of the dependent variable at various grid points.

II.4.1.3 Boundary and Initial Conditions

Boundary conditions (for spatial domains) and initial conditions (for time-dependent problems) are applied at the relevant grid points. These conditions offer insights into the system's behavior at the boundaries or during the initial time period.

II 4.1.4 Solution of the Discrete Equations

The set of discrete equations can be solved using numerical methods such as iterative approaches (such as Gauss-Seidel or Jacobi) or direct solvers (like LU decomposition). In this scenario, we select the LU decomposition method.

II.4.1.5 Post-processing and Analysis

Once the numerical solution is obtained, further processing of the data is conducted to extract pertinent information or conduct additional analysis. This could involve tasks such as visualizing the results, calculating derived parameters, or assessing the precision of the solution.

In summary, the mathematical representation of unsteady-state two-dimensional heat conduction without an internal heat source can be formulated as follows:

$$\frac{\partial^2 T}{\partial x^2} + \frac{\partial^2 T}{\partial y^2} = \frac{1}{\alpha}\frac{\partial T}{\partial t} \qquad \text{II 22}$$

With $\alpha = \frac{K}{\rho c_p}$ is the thermal diffusivity

Applying the first heat conduction equation in (II 22) to node (i, j) at time t, the equation can be rewritten as follows:

$$\left(\frac{\partial^2 T}{\partial x^2}+\frac{\partial^2 T}{\partial y^2}\right)_{i,j}^{t}=\frac{1}{\alpha}\left(\frac{\partial T}{\partial t}\right)_{i,j}^{t} \qquad \text{II 23}$$

The partial derivatives on both sides of equation (II 23) can be estimated using a difference quotient. The temperature component on the right-hand side of the equation can be approximated using a first-order difference quotient with respect to time.

$$\left(\frac{\partial T}{\partial t}\right)_{i,j}^{t}=\frac{T_{i,j}^{t+1}-T_{i,j}^{t}}{\Delta t} \qquad \text{II 24}$$

The second-order partial derivative on the left side of the equation (II 23) can be approximated using either an explicit or implicit method.

II.4.2 Types of Finite Difference Methods

II. 4.2.1 Explicit Method

The explicit method is a numerical technique used to solve partial differential equations (PDEs), particularly in the context of heat conduction problems. It is one of the simplest and most straightforward approaches to discretize and solve PDEs.

In this method, the solution for the current time step is directly calculated from the known values of the previous time step. It is simple to implement, but it can face stability challenges, especially with problems that exhibit rapid changes or are highly sensitive to initial conditions.

$$\left(\frac{\partial^2 T}{\partial x^2}+\frac{\partial^2 T}{\partial y^2}\right)_{i,j}^{t}=\frac{T_{i-1,j}^{t}-2T_{i,j}^{t}+T_{i+1,j}^{t}}{\Delta x^2}+\frac{T_{i,j-1}^{t}-2T_{i,j}^{t}+T_{i,j+1}^{t}}{\Delta y^2} \qquad \text{II 25}$$

Substituting (II 24) and (II 25) into (II 23) and taking $\Delta x=\Delta y$, we can write the total equation as follows:

$$\frac{T_{i,j}^{t+1}-T_{i,j}^{t}}{\Delta t}=\alpha\frac{-4T_{i,j}^{t}+T_{i+1,j}^{t}+T_{i-1,j}^{t}+T_{i,j-1}^{t}+T_{i,j+1}^{t}}{\Delta x^2} \qquad \text{II 26}$$

II. 4.2.2 Implicit Method

The implicit method is a numerical technique used to solve differential equations, particularly useful in time-dependent problems like heat conduction. Unlike the explicit method, the implicit method involves solving a system of equations at each time step, where the solution at the next time step depends on both the current and future values. This typically requires solving a set of simultaneous algebraic equations.

In this approach, the solution requires determining unknown values at the current time step (t) as well as the future state (t+1), necessitating the resolution of a system of equations. Implicit methods tend to be more stable but involve solving more extensive systems of equations.

Thus, we can write the following for the problem in question.

$$\left(\frac{\partial^2 T}{\partial x^2}+\frac{\partial^2 T}{\partial y^2}\right)_{i,j}^{t}=\frac{T_{i-1,j}^{t+1}-2T_{i,j}^{t+1}+T_{i+1,j}^{t+1}}{\Delta x^2}+\frac{T_{i,j-1}^{t+1}-2T_{i,j}^{t+1}+T_{i,j+1}^{t+1}}{\Delta y^2} \qquad \text{II 27}$$

Substituting (II 24) and (II 27) into (II 23) and taking $\Delta x=\Delta y$, we can write the total equation as follows:

$$\frac{T_{i,j}^{t+1}-T_{i,j}^{t}}{\Delta t}=\alpha\frac{-4T_{i,j}^{t+1}+T_{i+1,j}^{t+1}+T_{i-1,j}^{t+1}+T_{i,j-1}^{t+1}+T_{i,j+1}^{t+1}}{\Delta x^2} \qquad \text{II 28}$$

II.5 Nodal Energy Balance Equations

The nodal energy balance equation is a crucial tool in analyzing heat transfer processes. It applies the principle of energy conservation to a discrete point, or "node," within a thermal system.

Energy Conservation: The equation is based on the law of conservation of energy, which states that energy cannot be created or destroyed, only transferred or converted. At a node in a thermal system, this means the energy entering the node minus the energy leaving the node must equal the change in energy stored at the node over time.

Net Heat Transfer: The net rate of heat transfer into a node includes all forms of heat transfer:

Conduction: Heat transfer due to temperature between contacting surfaces.

Convection: Heat transfer between a solid surface and a fluid moving past the surface.

Radiation: Heat transfer through electromagnetic waves, such as the infrared radiation emitted by hot surfaces and solar irradiaton.

Rate of Change of Energy Stored: The energy stored at a node changes over time due to the heat entering and leaving. This change in stored energy is typically expressed as a time derivative of the node's temperature, multiplied by the node's heat capacity (a product of mass and specific heat).

II.5.1.Mesh study

Table: Outlet fluid temperature for different time step/space

Δt (s) / Δx (m)	**1920**	**960**	**480**	**240**	**120**	**60**
3/ **0.025**	85,4908	92,4555	92,5664	92,5640	92,5640	92,5640
5/ **0.0125**	85,4591	92,6780	92,8180	92,8156	92,8155	92,8155
6/ **0.01**	85,4626	92,7318	92,8781	92,8757	92,8757	92,8757
9/ **0.00625**	85,4742	92,8182	92,9744	92,9720	92,9719	
11/ **0.005**	85,4797	92,8485	93,0081	93,0057	93,0057	
17/**0.003125**	85,4896	92,9855	93,0602			

ΔT with refining time step

Δt (s) / Δx (m)	**1920**	ΔT **(K)**	**960**	ΔT **(K)**	**480**	ΔT **(K)**	**240**	ΔT **(K)**	**120**	ΔT **(K)**	**60**

3/ **0.025**	85,4908	6,9647	92,4555	0,1109	92,5664	0,0024	92,5640	0	92,5640	0	92,5640
5/ **0.0125**	85,4591	7,2189	92,6780	0,14	92,8180	0,0024	92,8156	0,0001	92,8155	0	92,8155
6/ **0.01**	85,4626	7,2692	92,7318	0,1463	92,8781	0,0024	92,8757	0	92,8757	0	92,8757
9/ **0.00625**	85,4742	7,344	92,8182	0,1562	92,9744	0,0024	92,9720	0,0001	92,9719	0	92,9719
11/ **0.005**	85,4797	7,3691	92,8485	0,1596	93,0081	0,0024	93,0057	0	93,0057		93,0057
17/**0.003125**	85,4896	7,4959	92,9855	0,0747	93,0602	0,0024	93,0626	0	93,0626	0	93,0626

ΔT with refining spase step

Δt (s) / Δx (m)	**1920**	**960**	**480**	**240**	**120**	**60**
3/ **0.025**	85,4908	92,4555	92,5664	92,5640	92,5640	92,5640
ΔT (K)	0,0317	0,2225	0,2516	0,2516	0,2515	0,2515
5/ **0.0125**	85,4591	92,6780	92,8180	92,8156	92,8155	92,8155
ΔT (K)	0,0035	0,0538	0,0601	0,0601	0,0602	0,0602
6/ **0.01**	85,4626	92,7318	92,8781	92,8757	92,8757	92,8757
ΔT (K)	0,116	0,0864	0,0963	0,0963	0,0962	0,0962
9/ **0.00625**	85,4742	92,8182	92,9744	92,9720	92,9719	92,9719
ΔT (K)	0,0055	0,0303	0,0337	0,0337	0,0338	0,0338
11/ **0.005**	85,4797	92,8485	93,0081	93,0057	93,0057	93,0057
ΔT (K)	0,0072	0,137	0,0521	0,0569	0,0569	0,0569
17/**0.003125**	85,4896	92,9855	93,0602	93,0626	93,0626	93,0626

After the comparison between the ΔTs we select the following mesh

Δx (m)=0.00625

Δt (s) =480

II.5.2 Data Entry:

Spesific Biot number $B_{iU} = \frac{U_L \Delta x}{K}$ II 29

Biot number $B_i = \frac{h_T \Delta x}{K}$ II 30

Fourier number $F_0 = \alpha \frac{\Delta t}{\Delta x^2}$ II 31

Thermal diffusivity $\alpha = \frac{K}{\rho c_p}$ II 32

$$C_1=\frac{B_{iU}.\Delta x.T_a}{e}+\frac{\tau.\alpha.I.\Delta x^2}{K.e} \quad \text{II 33}$$

$$C_2={}^{1}/_{F_0}+\frac{B_{iU}.\Delta x}{e}+4 \quad \text{II 34}$$

$$C_3=\frac{B_i(NY)}{N} \quad \text{II 35}$$

$$C_4=\frac{B_i(1)}{N} \quad \text{II 36}$$

where N is the number of risers

$$C_5=\frac{(N+1)B_i(NY)}{N} \quad \text{II 37}$$

$$C_6=\frac{(N+1)B_i(1)}{N} \quad \text{II 38}$$

$$C_7=B_i(i) \quad \text{II 39}$$

Were e is the plate theckness

Condition of equality of Nu:

$$\begin{cases}\dot{m}_T = N.\dot{m}_r \\ Re_T = Re_r\end{cases} \quad \text{II 40}$$

$\dot{m} = \rho AV$ and $A = \frac{\pi D^2}{4}$ where $\dot{m}$ is the mass flow rate and A is the cross-section area

$$R_e = \frac{\rho VD}{\mu}$$

$$\begin{cases}D_T^2.V_T = N.D_r^2.V_r \\ V_T.D_T = V_r.D_r\end{cases} \quad \text{II 41}$$

$$\left.\begin{cases}D_T = N.D_r \\ V_r = N.V_T\end{cases}\right\} \Rightarrow \quad h_r = N.h_T \quad \text{II 42}$$

Were D_T, V_T, h_T the diameter and fluid velocity and heat transfer coefficient in the manifold respectively

And D_r, V_r, h_r the diameter and fluid velocity and heat transfer coefficient in the riser respectively

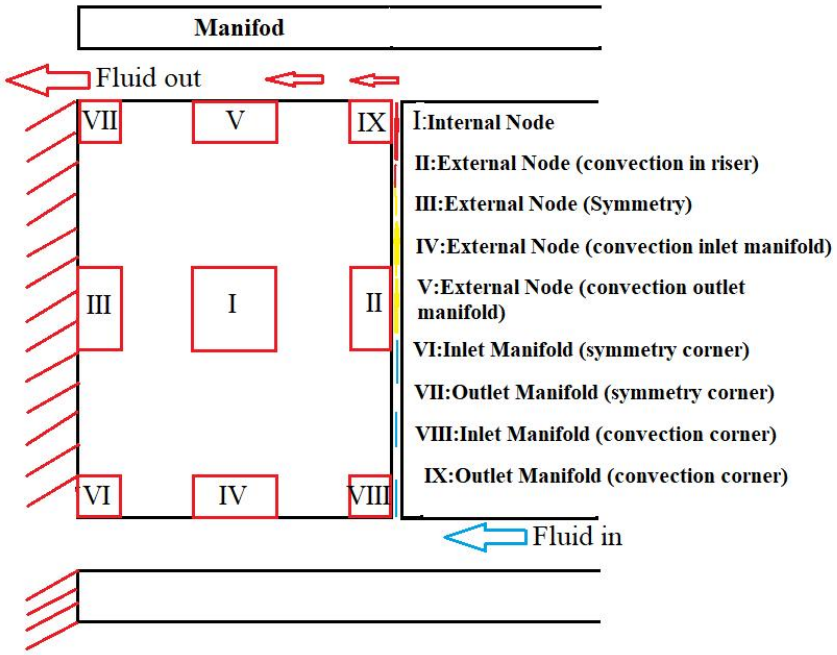

Figure II 5: Discretization scheme of the absorber plate

Figure II 5 illustrating the nine types of nodes based on their location. It should be noted that the actual number of nodes is significantly greater than those depicted.

II.5.3 Internal Node

Thermal balance of an internal node is:

$$Q_{cond} + Q_{irra} - Q_{loss} = mc_p \frac{dT}{dt} \qquad \text{II 43}$$

Assuming no heat generation inside the system equation II 43 becomes:

$$-K(\Delta ye)\frac{T_{i,j}^{t+\Delta t}-T_{i-1,j}^{t+\Delta t}}{\Delta x}-K(\Delta ye)\frac{T_{i,j}^{t+\Delta t}-T_{i+1,j}^{t+\Delta t}}{\Delta x}-K(\Delta xe)\frac{T_{i,j}^{t+\Delta t}-T_{i,j-1}^{t+\Delta t}}{\Delta y}-K(\Delta xe)\frac{T_{i,j}^{t+\Delta t}-T_{i,j+1}^{t+\Delta t}}{\Delta y}+\tau\alpha I.\Delta x\Delta y-$$
$$U_L\Delta x\Delta y\left(T_{i,j}^{t+\Delta t}-T_a\right)=(\rho\Delta x\Delta ye)c_p\frac{T_{i,j}^{t+\Delta t}-T_{i,j}^{t}}{\Delta t} \qquad \text{II 44}$$

With m= ρv= $\rho\Delta x\Delta ye$ and T_a is the ambient temperature and Δxe is the conduction area and $\Delta x\Delta y$ is the Solar irradiation receiving area. With $\Delta x=\Delta y$ the equation II 44 becomes:

$$C_2.T_{ij}^{t+dt}-\left(T_{i-1j}^{t+dt}+T_{i+1j}^{t+dt}+T_{ij-1}^{t+dt}+T_{ij+1}^{t+dt}\right)=C_1+\frac{T_{ij}^{t}}{F_0} \qquad \text{II 45}$$

II.5.4 External Node (convection in riser)

Thermal balance of the external node (convection in rise) is:

$$Q_{cond}+Q_{conv}+Q_{irra}-Q_{loss}=mc_p\frac{dT}{dt} \qquad \text{II 46}$$

With no heat generation inside the system equation II 46 will be as follows :

$$-K(\Delta ye)\frac{T_{i,j}^{t+\Delta t}-T_{i+1,j}^{t+\Delta t}}{\Delta x}-K(\Delta xe)\frac{T_{i,j}^{t+\Delta t}-T_{i,j-1}^{t+\Delta t}}{\Delta y}-K(\Delta xe)\frac{T_{i,j}^{t+\Delta t}-T_{i,j+1}^{t+\Delta t}}{\Delta y}-h_r(\Delta ye)\left(T_{i,j}^{t+\Delta t}-T_{fi}\right)+\tau\alpha I.\Delta x\Delta y-$$
$$U_L\Delta x\Delta y\left(T_{i,j}^{t+\Delta t}-T_a\right)=(\rho\Delta x\Delta ye)c_p\frac{T_{i,j}^{t+\Delta t}-T_{i,j}^{t}}{\Delta t} \qquad \text{II 47}$$

With T_f is the fluid temperature and Δye is the convection area. With $\Delta x=\Delta y$ the equation II 47 becomes:

$$(C_2+C_7).T_{ij}^{t+dt}-\left(2T_{i+1j}^{t+dt}+T_{ij-1}^{t+dt}+T_{ij+1}^{t+dt}\right)=C_1+C_7.T_{fi}+\frac{T_{ij}^{t}}{F_0} \qquad \text{II 48}$$

II.5.5 External Node (Symmetry)

Thermal balance of the external node (Symmetry) is the same as the internal node (II 43):

$$Q_{cond}+Q_{irra}-Q_{loss}=mc_p\frac{dT}{dt}$$

With no heat generation inside the system equation II 43 will be as follows :

$$-K(\Delta ye)\frac{T_{i,j}^{t+\Delta t}-T_{i-1,j}^{t+\Delta t}}{\Delta x}-K\left(\frac{\Delta x}{2}e\right)\frac{T_{i,j}^{t+\Delta t}-T_{i,j-1}^{t+\Delta t}}{\Delta y}-K\left(\frac{\Delta x}{2}e\right)\frac{T_{i,j}^{t+\Delta t}-T_{i,j+1}^{t+\Delta t}}{\Delta y}+\tau\alpha I.\frac{\Delta x}{2}\Delta y-U_L\frac{\Delta x}{2}\Delta y\left(T_{i,j}^{t+\Delta t}-T_a\right)=(\rho\frac{\Delta x}{2}\Delta ye)c_p\frac{T_{i,j}^{t+\Delta t}-T_{i,j}^{t}}{\Delta t} \quad \text{II 49}$$

With $\Delta x=\Delta y$ the equation II 49 becomes:

$$C_2.T_{ij}^{t+dt}-\left(2.T_{i-1j}^{t+dt}+T_{ij-1}^{t+dt}+T_{ij+1}^{t+dt}\right)=C_1+\frac{T_{ij}^{t}}{F_0} \quad \text{II 50}$$

II.5.6 External Node (convection in manifold)

Thermal balance of the external node (convection in manifold) is the same external node (convection in riser) (II 46):

$$Q_{cond}+Q_{conv}+Q_{irra}-Q_{loss}=mc_p\frac{dT}{dt}$$

II.5.6.1 Inlet Manifold

With no heat generation inside the system equation II 46 will be as follows :

$$-K\left(\frac{\Delta y}{2}e\right)\frac{T_{i,j}^{t+\Delta t}-T_{i-1,j}^{t+\Delta t}}{\Delta x}-K\left(\frac{\Delta y}{2}e\right)\frac{T_{i,j}^{t+\Delta t}-T_{i+1,j}^{t+\Delta t}}{\Delta x}-K(\Delta xe)\frac{T_{i,j}^{t+\Delta t}-T_{i,j+1}^{t+\Delta t}}{\Delta y}-h_T(\Delta xe)\left(T_{i,j}^{t+\Delta t}-T_{f1}\right)+\tau\alpha I.\frac{\Delta x^2}{2}-U_L\frac{\Delta x^2}{2}\left(T_{i,j}^{t+\Delta t}-T_a\right)=\left(\rho\frac{\Delta x^2}{2}e\right)c_p\frac{T_{i,j}^{t+\Delta t}-T_{i,j}^{t}}{\Delta t} \quad \text{II 51}$$

With $h_T=\frac{h_r}{N}$ II 51 becomes:

$$(C_2+C_4).T_{ij}^{t+dt}-\left(T_{i-1j}^{t+dt}+T_{i+1j}^{t+dt}+2.T_{ij+1}^{t+dt}\right)=C_1+C_4.T_{f1}+\frac{T_{ij}^{t}}{F_0} \quad \text{II 52}$$

II.5.6.2 Outlet Manifold

$$-K\left(\frac{\Delta y}{2}e\right)\frac{T_{i,j}^{t+\Delta t}-T_{i-1,j}^{t+\Delta t}}{\Delta x}-K\left(\frac{\Delta y}{2}e\right)\frac{T_{i,j}^{t+\Delta t}-T_{i+1,j}^{t+\Delta t}}{\Delta x}-K(\Delta xe)\frac{T_{i,j}^{t+\Delta t}-T_{i,j-1}^{t+\Delta t}}{\Delta y}-h_T(\Delta xe)\left(T_{i,j}^{t+\Delta t}-T_{fNY}\right)+\tau\alpha I.\frac{\Delta x^2}{2}-U_L\frac{\Delta x^2}{2}\left(T_{i,j}^{t+\Delta t}-T_a\right)=\left(\rho\frac{\Delta x^2}{2}e\right)c_p\frac{T_{i,j}^{t+\Delta t}-T_{i,j}^{t}}{\Delta t} \quad \text{II 53}$$

With $h_T=\frac{h_r}{N}$ equation II 51 becomes:

$$(C_2 + C_3).T_{ij}^{t+dt} - \left(T_{i-1j}^{t+dt} + 2.T_{ij-1}^{t+dt} + T_{i+1j}^{t+dt}\right) = C_1 + C_3.T_f(NY) + \frac{T_{ij}^{t}}{F_0} \qquad \text{II 54}$$

II.5.6.3 Inlet Manifold (symmetry corner)

$$-K\left(\frac{\Delta y}{2}e\right)\frac{T_{i,j}^{t+\Delta t} - T_{i-1,j}^{t+\Delta t}}{\Delta x} - K\left(\frac{\Delta x}{2}e\right)\frac{T_{i,j}^{t+\Delta t} - T_{i,j+1}^{t+\Delta t}}{\Delta y} - h_T\left(\frac{\Delta x}{2}e\right)\left(T_{i,j}^{t+\Delta t} - T_{f1}\right) + \tau\alpha I.\frac{\Delta x^2}{4} - U_L\frac{\Delta x^2}{4}\left(T_{i,j}^{t+\Delta t} - T_a\right) = \left(\rho\frac{\Delta x^2}{4}e\right)c_p\frac{T_{i,j}^{t+\Delta t} - T_{i,j}^{t}}{\Delta t} \qquad \text{II 55}$$

then

$$(C_2 + C_4).T_{ij}^{t+dt} - 2\left(T_{i-1j}^{t+dt} + T_{ij+1}^{t+dt}\right) = C_1 + C_4.T_f(1) + \frac{T_{ij}^{t}}{F_0} \qquad \text{II 56}$$

II 5.6.4 Outlet Manifold (symmetry corner)

$$-K\left(\frac{\Delta y}{2}e\right)\frac{T_{i,j}^{t+\Delta t} - T_{i-1,j}^{t+\Delta t}}{\Delta x} - K\left(\frac{\Delta x}{2}e\right)\frac{T_{i,j}^{t+\Delta t} - T_{i,j-1}^{t+\Delta t}}{\Delta y} - h_T\left(\frac{\Delta x}{2}e\right)\left(T_{i,j}^{t+\Delta t} - T_{fNY}\right) + \tau\alpha I\frac{\Delta x^2}{4} - U_L\frac{\Delta x^2}{4}\left(T_{i,j}^{t+\Delta t} - T_a\right) = \left(\rho\frac{\Delta x^2}{4}e\right)c_p\frac{T_{i,j}^{t+\Delta t} - T_{i,j}^{t}}{\Delta t} \qquad \text{II 57}$$

then

$$(C_2 + C_3).T_{ij}^{t+dt} - 2\left(T_{i-1j}^{t+dt} + T_{ij-1}^{t+dt}\right) = C_1 + C_3.T_f(NY) + \frac{T_{ij}^{t}}{F_0} \qquad \text{II 58}$$

II.5.6.5 Inlet Manifold (convection corner):

$$-K\left(\frac{\Delta y}{2}e\right)\frac{T_{i,j}^{t+\Delta t} - T_{i+1,j}^{t+\Delta t}}{\Delta x} - K\left(\frac{\Delta x}{2}e\right)\frac{T_{i,j}^{t+\Delta t} - T_{i,j+1}^{t+\Delta t}}{\Delta y} - (h_T + h_r)\left(\frac{\Delta x}{2}e\right)\left(T_{i,j}^{t+\Delta t} - T_{f1}\right) + \tau\alpha I.\frac{\Delta x^2}{4} - U_L\frac{\Delta x^2}{4}\left(T_{i,j}^{t+\Delta t} - T_a\right) = \left(\rho\frac{\Delta x^2}{4}e\right)c_p\frac{T_{i,j}^{t+\Delta t} - T_{i,j}^{t}}{\Delta t} \qquad \text{II 59}$$

then

$$(C_2 + C_6).T_{ij}^{t+dt} - 2\left(T_{i+1j}^{t+dt} + T_{ij+1}^{t+dt}\right) = C_1 + C_6.T_f(1) + \frac{T_{ij}^{t}}{F_0} \qquad \text{II 60}$$

II.5.6.6 Outlet Manifold (convection corner)

$$-K\left(\frac{\Delta y}{2}e\right)\frac{T_{i,j}^{t+\Delta t}-T_{i+1,j}^{t+\Delta t}}{\Delta x}-K\left(\frac{\Delta x}{2}e\right)\frac{T_{i,j}^{t+\Delta t}-T_{i,j-1}^{t+\Delta t}}{\Delta y}-(h_T+h_r)\left(\frac{\Delta x}{2}e\right)\left(T_{i,j}^{t+\Delta t}-T_{fNY}\right)+\tau\alpha I\frac{\Delta x^2}{4}-U_L\frac{\Delta x^2}{4}\left(T_{i,j}^{t+\Delta t}-T_a\right)=\left(\rho\frac{\Delta x^2}{4}e\right)c_p\frac{T_{i,j}^{t+\Delta t}-T_{i,j}^{t}}{\Delta t} \quad \text{II 61}$$

II 61 becomes :

$$(C_2+C_5).T_{ij}^{t+dt}-2\left(T_{i+1j}^{t+dt}+T_{ij-1}^{t+dt}\right)=C_1+C_5.T_f(NY)+\frac{T_{ij}^{t}}{F_0} \quad \text{II 62}$$

II.6 The Program Algorithm

The developed program is inspired by the work of Rahal.A and Khalifa med. A [47] it is composed of the following parts.

II.6.1 Data Entry

The length , width , number of risers, initial temperature of the solid, initial temperature of the fluid, air density, specific heat and density of fluid, specific heat of solid, number of time iterations, thermal conductivity, fluid mass flow , riser and manifold diameter, dynamic viscosity, Kinematic Viscosity of air.

II.6.2. Calculation of Constants

The step of space: $\Delta x=\Delta y=\frac{w}{NX-1}=\frac{L}{NY-1}$

The thermal diffusivity α by the equation: $\alpha=\frac{K}{\rho c_p}$

The Fourier number $F_0=\alpha\frac{\Delta t}{\Delta x^2}$

The fluid velocity $V=\frac{\dot{m}}{\rho A}$

II.6.3. The Initial Temperature of the Solid

All nodes of solid are equal to Ti at t=0s

II.6.4. Riser Fluid Temperature

The temperature changes from one node to another and is calculated using equation II 11

To calculate and use equation II.11 between two nodes, the equation II.11 must be adjusted. The temperature between two adjacent nodes is assumed to be constant since the nodes are very close to each other and the temperature difference is minimal.

$$T_{fi+1} = \left(\mathrm{T}_{fi} - \mathrm{Tw}\right) e^{-\frac{\pi D h \Delta x}{\dot{m} c_p}} + \mathrm{Tw} \qquad \text{II 63}$$

With $T_w = \frac{T_i + T_{i+1}}{2}$

Tw: the mean temperature of tow adjacent nodes (considered as constat).

The Locale Reynolds number, Prandt number and Nusselt number :

$\mathrm{Re} = \frac{\rho V D}{\mu}$

$\mathrm{Pr} = \frac{C_p \mu}{K}$

$\mathrm{Nu} = \frac{hD}{K}$

If Re<2300 so Nu=4.36
If not so

$\mathrm{Nu}=0.023*(\mathrm{Re}^{0.8})*(\mathrm{Pr}^{(1/3)})$;

The locale convection coefficient and Biot number

$h_r = \frac{\mathrm{Nu}K}{D}$

$B_i = \frac{h_r \Delta x}{K}$

II.6.5. Calculation of Number of Iterations

In the studied case we have 2 hours to be considered

2 hours =7200 s

P= 7200/dt represent the number of iterations

II.6.6. Absorber Plate Temperature Calculation

The temperature of internal nodes are calculated using equation II 45

The temperature of convection in riser nodes are calculated using equation II 48

The temperature of Symmetry nodes are calculated using equation II 50

The temperature of Inlet Manifold nodes are calculated using equation II 52

The temperature of Outlet Manifold nodes are calculated using equation II 54

The temperature of Inlet Manifold (symmetry corner) nodes are calculated using equation II 56

The temperature of Outlet Manifold (symmetry corner) nodes are calculated using equation II 58

The temperature of Inlet Manifold (convection corner) nodes are calculated using equation II 60

The temperature of Outlet Manifold (convection corner) nodes are calculated using equation II 62

Flowchart for the algorithm

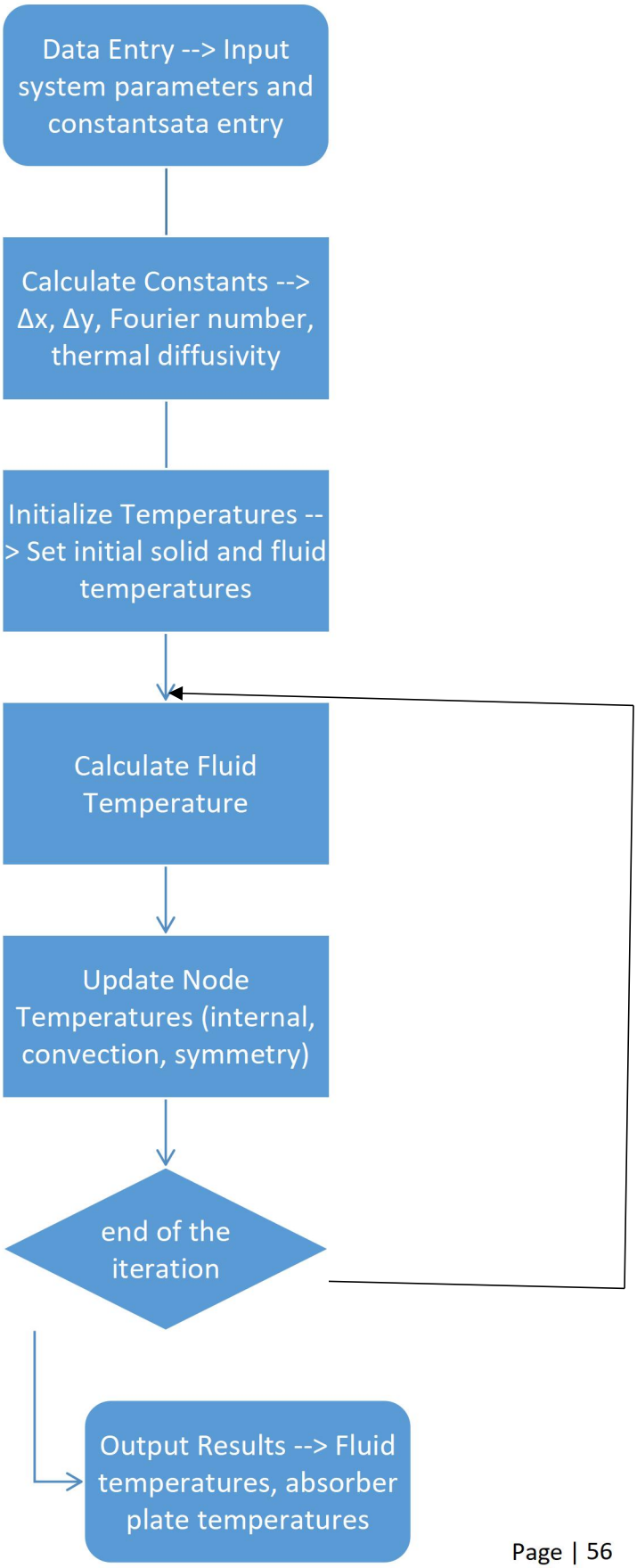
Data Entry --> Input system parameters and constantsata entry
Calculate Constants --> Δx, Δy, Fourier number, thermal diffusivity
Initialize Temperatures --> Set initial solid and fluid temperatures
Calculate Fluid Temperature
Update Node Temperatures (internal, convection, symmetry)
end of the iteration
Output Results --> Fluid temperatures, absorber plate temperatures

II.7 Conclusion

In conclusion, flat plate solar collectors (FPSC) are effective devices for harnessing solar energy and converting it into usable heat, primarily for applications like water heating or space heating. Their design typically includes components like the absorber plate, transparent cover, and an insulation layer to minimize heat losses while optimizing energy absorption. The efficiency of FPSCs depends on factors such as material properties, the design of the absorber, and heat transfer mechanisms like conduction, convection, and radiation.

Flat plate solar collectors are reliable, cost-effective, and have been widely adopted in regions with abundant solar radiation. Their design simplicity and relatively low maintenance make them a popular choice in both residential and commercial settings. Advanced numerical models and heat transfer analyses, like those discussed in calculation models, play a key role in enhancing their performance by predicting temperature distributions and heat gains, leading to better design optimization.

Introduction

This chapter presents a detailed analysis of the simulation results obtained from the numerical model developed for the thermal performance of flat plate solar collectors (FPSCs). The main objective is to evaluate the effect of various parameters, including mass flow rate, riser length, and solar irradiance, on the thermal efficiency and temperature distribution of the system.

The chapter begins with a discussion of the temperature contours over different time intervals, illustrating how the temperature evolves across the absorber plate. This is followed by a thorough examination of the impact of different mass flow rates on the performance of the FPSC, providing insights into the relationship between flow dynamics and heat transfer efficiency. Additionally, the influence of riser length and solar irradiance on the outlet fluid temperature and system efficiency is explored in detail.

Through these analyses, the chapter aims to highlight the key factors that influence the performance of flat plate solar collectors, guiding future improvements in solar thermal system design.

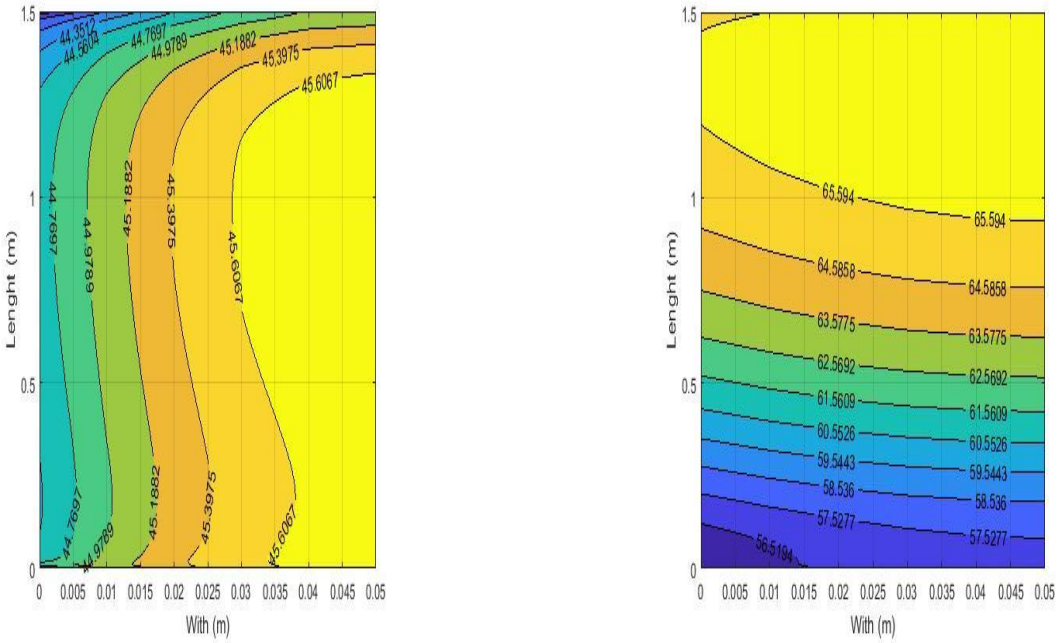

III.1 Temperature Contour for Different Timesteps

a. t= 8 min

b. t= 16 min

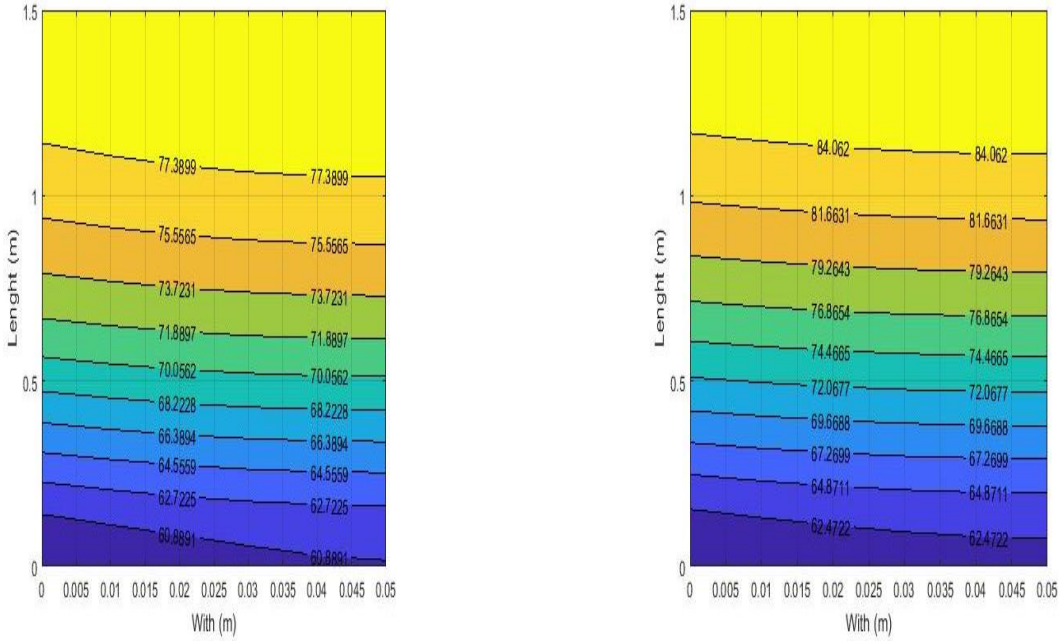

c. t= 24 min

d. t= 32 min

Figure III 1 Temperature Contour for different timesteps

Figure III-1 presents the absorber plate temperature contour, which is a graphical representation of two-dimensional surface using contour lines. In these figures, the plot shows how the temperature (represented by the contour lines) varies across two dimensions; width and length of the absorber plate in unsteady state. such a representation is impossible in the analytical calculation.

III.2 Impact of the Mass flow

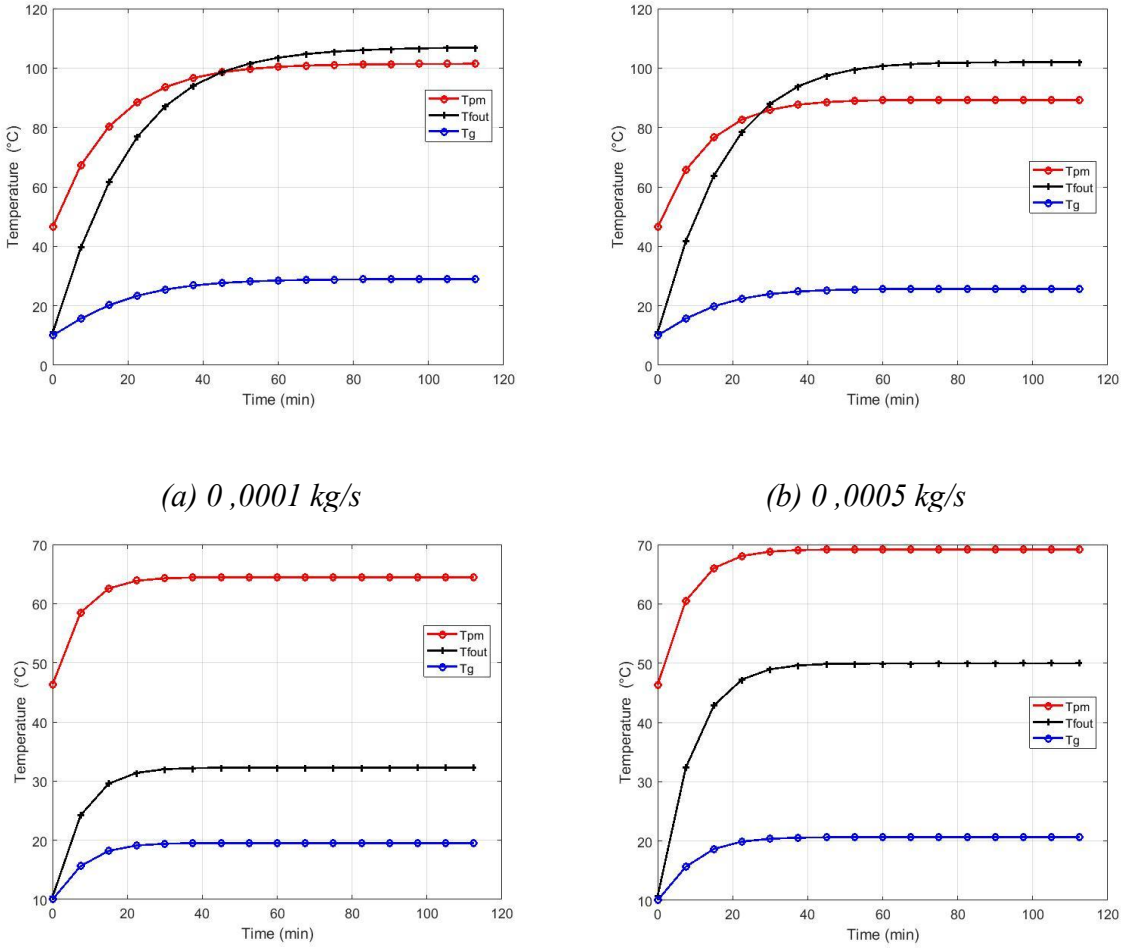

(a) 0 ,0001 kg/s *(b) 0 ,0005 kg/s*

(c) 0 ,005 kg/s *(d) 0 ,0025 kg/s*

Figure III 2 Variation of temperature for different mass flow

Figure III 2 (a, b, c, and d) depicts the temperature change for the outlet fluid, mean plate, and glass cover at various mass flow rates we maintain the length and the solar irradiance

constant as 1m; 1000 W/m² respectively. At the mass flow of 0.0001 kg/s, the mean plate temperature starts at 47°C, increases rapidly, and stabilizes around 101°C after approximately 80 minutes. The outlet fluid temperature begins at 10°C and rises more slowly, reaching a steady temperature of about 107°C after 100 minutes. The glass cover temperature increases steadily but remains lower than both the mean plate and outlet fluid temperatures, stabilizing at around 25°C.

For 0.0005 kg/s, the mean plate temperature starts at 46°C, rises quickly, and levels off at approximately 88°C after 60 minutes. The outlet fluid temperature begins at 10°C and climbs more slowly, stabilizing around 101°C after 80 minutes. The glass cover temperature rises consistently, settling at about 20°C. At 0.005 kg/s, the mean plate temperature starts at 47°C, increases rapidly, and stabilizes at around 64°C after 40 minutes. The outlet fluid temperature begins at 10°C, rises more slowly than the mean plate temperature, and stabilizes around 32°C after 40 minutes. The glass cover temperature steadily increases but stays below both the mean plate and outlet fluid temperatures, reaching about 20°C.

For 0.0025 kg/s, the mean plate temperature starts at 47°C, increases quickly, and stabilizes at approximately 69°C after 40 minutes. The outlet fluid temperature begins at 10°C, rises more slowly, and reaches a steady state near 50°C after 40 minutes. The glass cover temperature increases steadily but remains below both the mean plate and outlet fluid temperatures, stabilizing at around 20°C.

III.3 Impact of Riser Length

Figure III 3 (a, b, c, and d) shows the outlet fluid, mean plate and glass cover temperature for different length of the riser we maintain the mass flow and the solar irradiance constant as 0.001 kg/s ; 1000 W/m² respectively. For the length of 1m, the value of mean plate temperature begins at 47°C and rises quickly until it stabilize near 75°C after approximately 40 minutes. The outlet fluid temperature starts low at 10 °C and increases gradually compared to mean plate temperature, reaching a steady state temperature of around 68°C after 60 minutes. The glass cover temperature follow a constant increase but remains below

both mean plate temperature and outlet fluid temperature, and stabilizing at around 22°C. and for the length of 1.5m, the value of mean plate temperature Starts at 47°C and rapidly increases, stabilizing at around 80°C after 60 minutes. The outlet fluid temperature begins at 10°C and climbs more slowly than mean plate temperature, reaching a stable temperature of about 83°C after 68 minutes. The glass cover temperature rises, leveling off at approximately 24°C.

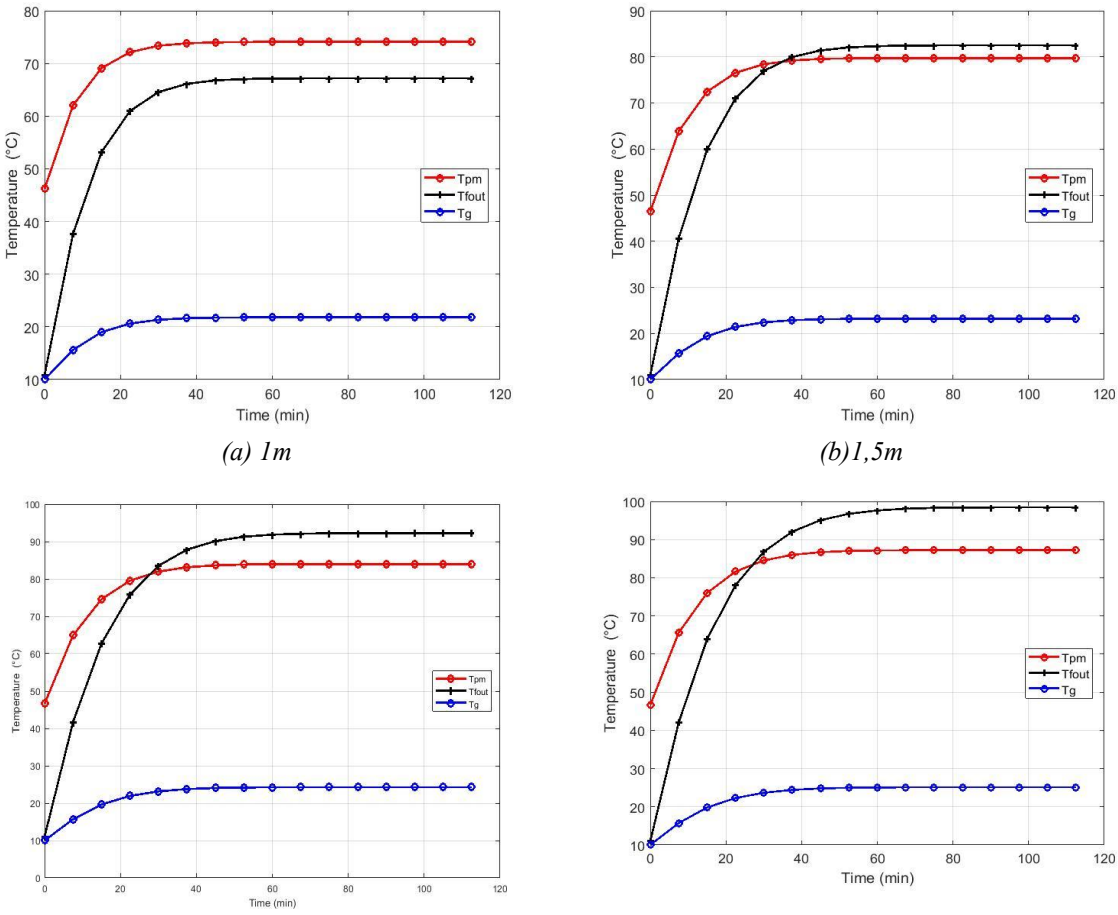

(a) 1m *(b)1,5m*

(c) 2m *(d)2,5m*

Figure III 3 Variation of temperature for different length

In case of 2m, the rate of mean plate temperature begins at 47°C and increases rapidly until it levels off near 84°C after about 60 minutes. The outlet fluid temperature starts at 10°C and rises more slowly compared to the mean plate temperature, eventually stabilizing

around 93°C after 60 minutes. The temperature of the glass cover increases steadily but stays below both the mean plate temperature and the outlet fluid temperature, reaching a steady value of approximately 25°C. For 2.5m, the rate of mean plate temperature starts at 47°C, rapidly increases, and then levels off at approximately 87°C after 60 minutes. The outlet fluid temperature begins at 10°C and rises more slowly than mean plate temperature, reaching a stable point near 99°C after 78 minutes. Meanwhile, The temperature of the glass cover rises steadily but stays below both mean plate temperature and The outlet fluid temperature, ultimately stabilizing at around 25°C.

III.4 Impact of Solar Irradiance

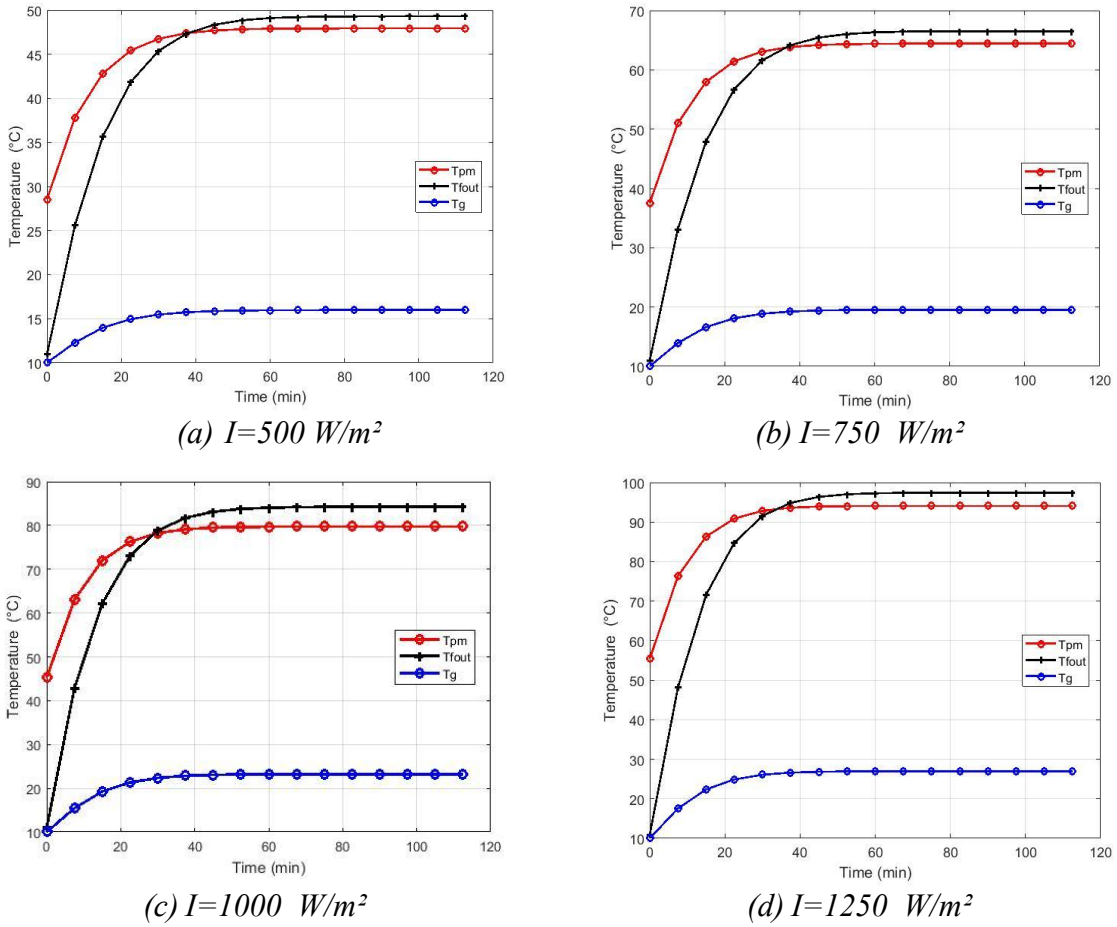

(a) I=500 W/m² *(b) I=750 W/m²*

(c) I=1000 W/m² *(d) I=1250 W/m²*

Figure III 4 Variation of temperature for different Solar Irradiance

Figure III 4 (a, b, c, and d) illustrates the temperature variations for the outlet fluid, mean plate, and glass cover across different Solar Irradiances we maintain the length and mass flow constant at 1m ; 0.001 kg/s respectively. At I=500 W/m², the mean plate temperature starts at 28°C, quickly climbs, and stabilizes around 47°C after about 48 minutes. The outlet fluid temperature begins at 11°C and increases more gradually, reaching a steady state of approximately 60°C after 60 minutes. The glass cover temperature rises consistently but remains below both the mean plate and outlet fluid temperatures, stabilizing at around 16°C. For I=750 W/m², the mean plate temperature starts at 38°C, rapidly rises, and levels off near 64°C after 45 minutes. The outlet fluid temperature starts at 10°C and climbs more slowly, reaching about 67°C after 60 minutes. The glass cover temperature increases steadily, stabilizing at around 20°C. At I=1000 W/m², the mean plate temperature starts at 46°C, rises quickly, and stabilizes at approximately 80°C after 45 minutes. The outlet fluid temperature begins at 10°C, increases more slowly than the mean plate temperature, and stabilizes around 84°C after 60 minutes. The glass cover temperature rises steadily but remains below both the mean plate and outlet fluid temperatures, reaching about 23°C.

For I=1250 W/m², the mean plate temperature starts at 56°C, increases rapidly, and stabilizes at approximately 94°C after 45 minutes. The outlet fluid temperature begins at 10°C and rises more slowly, reaching a steady state near 98°C after 60 minutes. The glass cover temperature rises consistently but stays below both the mean plate and outlet fluid temperatures, stabilizing at around 27°C.

III.5 Impact of Absorber Plate Material

In order to study the impact of the absorber plate material length, mass flow and the solar irradiance are maintained constant at 1.5m , 0.001 kg/s and 1000 W/m² respectively.

III.5.1 Copper Plate

Figure III.5 (Temperature variation for Copper Plate) displays the temperature variation of the glass cover, absorber plate (copper), and outlet fluid over time. Initially, the temperature of the glass cover starts low and gradually rises, remaining below both the plate and fluid

temperatures throughout the observation. The absorber plate (made of copper) shows a rapid increase in temperature initially, stabilizing after reaching a peak. The outlet fluid temperature also rises, following the copper plate temperature but at a slower rate, eventually reaching a steady state. The copper plate demonstrates efficient heat absorption, resulting in higher outlet fluid temperatures.

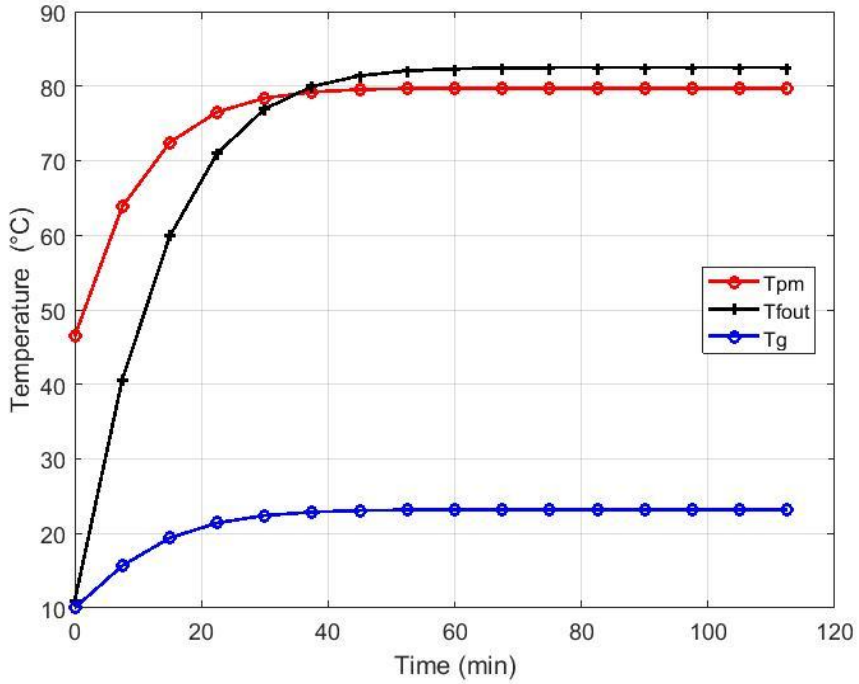

Figure III 5 Mean plate, outlet fluid and glass cover temperature as function of time

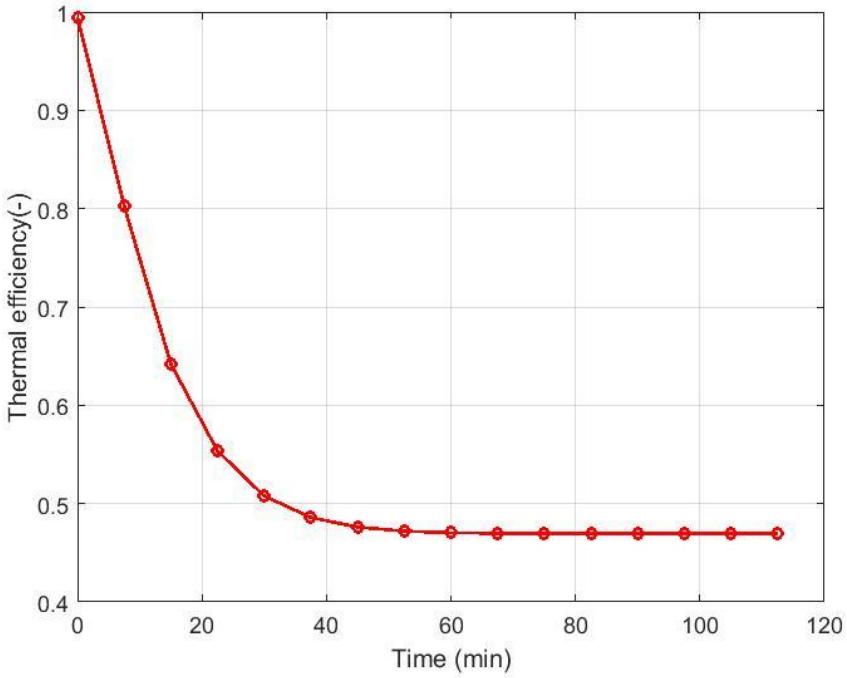

Figure III 6 Thermal efficiency as function of time

Figure III.6 (Thermal efficiency for Copper Plate**)** illustrates the thermal efficiency of the flat plate solar collector over time using a copper absorber plate. The graph shows that thermal efficiency starts higher and decreases steadily as the system reaches operational equilibrium. Once the temperatures stabilize, the efficiency curve flattens, indicating the optimal performance of the system using copper, which is a highly conductive material that enhances the heat transfer process.

III 5.2 AISI 304 Stailess Steel Plate:

Figure III.7 (Temperature variation for AISI 304 Stainless Steel Plate): This figure represents the temperature variation of the glass cover, absorber plate (stainless steel), and outlet fluid over time. Similar to the copper plate, the glass cover shows a gradual increase in temperature, staying lower than the plate and fluid temperatures.

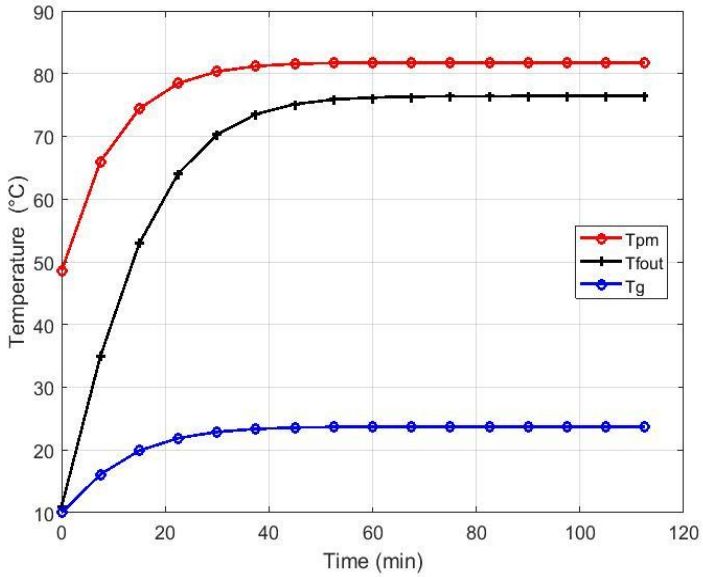

Figure III 7 Mean plate, outlet fluid and glass cover temperature as function of time

The stainless steel plate experiences a slower rise in temperature compared to copper, eventually stabilizing at a higher value. However, the outlet fluid temperature increases more slowly and stabilizes at a lower temperature than that observed with the copper plate, indicating less efficient heat transfer.

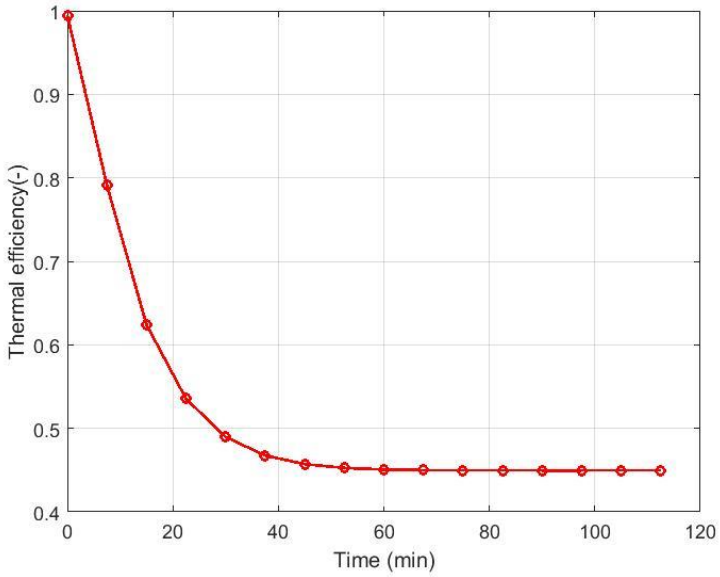

Figure III 8 Thermal efficiency as function of time

Figure III.8 (Thermal efficiency for AISI 304 Stainless Steel Plate) illustrates the thermal efficiency of the system using a stainless steel absorber plate. The thermal efficiency rises initially but stabilizes at a lower level compared to the copper plate. Despite the higher temperature of the stainless steel plate, the lower outlet fluid temperature suggests that stainless steel is less effective at transferring heat to the fluid, resulting in a lower overall thermal efficiency than the copper plate system.

These descriptions explain how the copper plate performs better in terms of heat transfer and efficiency compared to the stainless steel plate.

III. 6 Conclusion

The results presented in Chapter IV illustrate the performance of a flat plate solar collector (FPSC) under various conditions, including changes in mass flow rate, riser length, solar irradiance, and the material of the absorber plate.

The findings show that the mean plate and outlet fluid temperatures stabilize over time across different flow rates and riser lengths. For example, increasing the mass flow rate

reduces the plate temperature but increases the temperature stability of the outlet fluid. Similarly, longer riser lengths improve heat transfer, leading to higher outlet fluid temperatures.

Solar irradiance significantly impacts the temperature, with higher irradiance resulting in higher temperatures for both the plate and the fluid. Among the materials tested for the absorber plate, copper demonstrates superior performance in maintaining a higher outlet fluid temperature compared to stainless steel, making it the more efficient option.

In conclusion, the FPSC's performance is highly dependent on factors like mass flow rate, riser length, and solar irradiance. Copper is found to be the optimal absorber plate material due to its ability to achieve higher fluid outlet temperatures, enhancing thermal efficiency.

General Conclusion

The research on flat plate solar collectors (FPSCs) provides a comprehensive understanding of their design, operation, and optimization. FPSCs are essential in harnessing solar energy, a renewable and sustainable source of power, making them crucial in efforts to reduce carbon emissions and combat climate change. By absorbing solar radiation and converting it into usable heat energy, FPSCs serve critical functions in water heating, space heating, and other thermal applications in residential, commercial, and industrial settings.

Through numerical and analytical methods, significant improvements in the thermal efficiency of FPSCs have been achieved by optimizing design parameters and minimizing heat losses. Models developed in this study, incorporating principles of conduction, convection, and radiation, provide accurate predictions of FPSC behavior, allowing for better design and operational strategies.

The performance of FPSCs is influenced by several factors, including the mass flow rate, riser length, solar irradiance, and the material of the absorber plate. The use of copper as an absorber plate material demonstrates superior heat transfer capabilities and higher thermal efficiency compared to stainless steel, making it the better choice for achieving higher fluid outlet temperatures.

Flat plate solar collectors represent an efficient and reliable solution for solar thermal energy utilization. Their optimization through material selection and operational conditions can lead to substantial energy savings and environmental benefits. The advancement of analytical and numerical modeling techniques continues to enhance the design and efficiency of FPSCs, contributing to their increased adoption in sustainable energy systems worldwide.

References

[1] Duffie, J. A., & Beckman, W. A. (2013). Solar Engineering of Thermal Processes (4th ed.). John Wiley & Sons

[2] Tiwari, G. N., & Mishra, R. K. (2013). Solar Energy: Fundamentals, Design, Modelling, and Applications. Alpha Science International Ltd

[3] Hottel, H. C., & Whillier, A. (1955). Evaluation of Flat-Plate Solar Heat Collector. Transactions of the ASME, 77(4), 875-882. [Journal Article]

[4] Khan, M. Y., & Zubair, S. M. (2017). Solar Energy: Fundamentals, Design, Modeling and Applications. Springer. [Book]

[5] Kalogirou, S. A. (2009). Solar Energy Engineering: Processes and Systems. Academic Press. [Book]

[6] Duffie, J. A. (1960). Transient Heat Transfer in Flat-Plate Solar Collectors. Solar Energy, 4(3), 29-44. [Journal Article]

[7] Jordan, R. C., & Stine, W. B. (1987). Performance of Flat-Plate Solar-Collectors at Elevated Temperatures. Solar Energy, 38(2), 89-95. [Journal Article]

[8] Çengel, Y. A., & Boles, M. A. (2014). Thermodynamics: An Engineering Approach. McGraw-Hill Education.

[9] Patankar, S.V. (1980). Numerical Heat Transfer and Fluid Flow. Hemisphere Publishing Corporation.

[10] Kreith, F., & Kreider, J. F. (1978). *Principles of Solar Engineering*. McGraw-Hill.

[22] "BYJU'S," 2022. [Online]. Available: https://byjus.com/ncert-solutions-class-6/.

[23] Goswami, D. Y., Kreith, F., & Kreider, J. F. (2000). *Principles of Solar Engineering* (2nd ed.). Taylor & Francis.

[24] Tchanche F.B., Papadakis G., Lambrinos G., Frangoudakis A. Fluid selection for a low-temperature solar organic Rankine cycle. Appl. Therm. Eng. 2009;29:2468–2476.

[25] https://www.ncbi.nlm.nih.gov/pmc/articles/PMC8980339/#bib89

[26] https://www.mdpi.com/2071-1050/12/21/9119

[27] Chafie M., Ben Aissa M., Guizani A. Energetic end exergetic performance of a parabolic trough collector receiver: an experimental study. J. Clean. Prod. 2018;171:285–296.

[28] Romero M., González-Aguilar J. Solar thermal CSP technology. Wiley interdisciplinary reviews. *Energy Environ.* 2013;3(1):42–59.

[29] Achour L., Bouharkat M., Behar O. Performance assessment of an integrated solar combine cycle in the southern of Algeria. Energy Rep. 2018;(4):207–217.

[30] Kizilkan O., Nižetić S., Yildirim G. Energy Transport Global Warming; 2016. Solar Assisted Organic Rankine Cycle for Power Generation: a Comparative Analysis for Natural Working Fluids; pp. 175–192.

[31] Rosell J., Vallverdú X., Lechón M., Ibáñez M. Design and simulation of a low concentrating photovoltaic/thermal system. Energy Convers. Manag. 2005;46(18-19):3034–3046.

[32] Grena R., Tarquini P. Solar linear Fresnel collector using molten nitrates as heat transfer fluid. Energy. 2011;(36):1048–1056.

[33] Bellos E., Tzivanidis C., Papadopoulos A. Optical and thermal analysis of a linear Fresnel reflector operating with thermal oil, molten salt and liquid sodium. Appl. Therm. Eng. 2018;133:70–80.

[34] Gharbi N.E., Derbal H., Bouaichaoui S., Said N. A comparative study between parabolic trough collector and linear Fresnel reflector technologies. Energy Proc. 2011;(6):566–572.

[35] Mancini, T., Heller, P., Butler, B., et al. (2003). "Dish-Stirling Systems: An Overview of Development and Status." Journal of Solar Energy Engineering, 125(2), 135-144

[36] Madadi V., Rahimi A., Tavakoli T. First and second thermodynamic law analyses applied to a solar dish collector. J. Non-Equilibrium Thermodyn. 2014;39(4):183–197

[37] Rabbani M., Ratlamwala T.A.H., Dincer I. Development of a new heliostat field-based integrated solar energy system for cogeneration. Arabian J. Sci. Eng. 2017;43:1267–1277.

[38] Romero, M., & González-Aguilar, J. (2014). "Solar thermal CSP technology." Renewable Energy Sources and Climate Change Mitigation, 35, 283-296.

[39] Zambolin, E., & Del Col, D. (2010). "Experimental analysis of thermal performance of flat plate and evacuated tube solar collectors in stationary standard and daily conditions." Solar Energy, 84(8), 1382-1396.

[40] https://link.springer.com/article/10.1007/s10765-020-02737-1

[41] Kalogirou, S. A. (2004). "Solar thermal collectors and applications." Progress in Energy and Combustion Science, 30(3), 231-295.

[42] https://www.researchgate.net/figure/arious-types-of-solar-thermal-collectors-Concentration-ratio-has-been-abbreviated-as_fig21_322252433

[43] Kalogirou S. Solar energy engineering: processes and systems; London: Elsevier;2009.

[44] F. Kreith, R. M. Manglik and M. S. Bohn, Principales of heat transfer, Cengage Learning, 2011.

[45] C. H. forsberg, Heat Transfer principles and applications, Elsevier, 2021.

[46] C. H. forsberg, Heat Transfer principles and applications, Elsevier, 2021.

[47] E. C. F Rahal. A and Khalifa med. A Koumad. A. (2021). " Élaboration d'un Logiciel de Calcul de Stockage d'Energie Thermique Sensible".